Available online at www.sciencedirect.com
ScienceDirect
Coordination Chemistry Reviews 253 (2009) 1–20
COORDINATION CHEMISTRY REVIEWS
www.elsevier.com/locate/ccr

Review

Luminescent groups **10** and **11** heteropolynuclear complexes based on thiolate or alkynyl ligands

Zhong-Ning Chen *, Na Zhao, Yang Fan, Jun Ni

State Key Laboratory of Structural Chemistry, Fujian Institute of Research on the Structure of Matter, The Chinese Academy of Sciences, Fuzhou, Fujian 350002, China

Received 10 July 2007; accepted 19 November 2007
Available online 24 November 2007

Contents

Abstract

A family of groups **10** and **11** heteropolynuclear thiolate or alkynyl complexes has been prepared by incorporating d^8 or d^{10} metal thiolate/alkynyl species with d^{10} metal diphosphine components. This review article presents our recent progress in the design of luminescent d^8–d^{10} or d^{10}–d^{10} multicomponent and heteropolynuclear complexes based on thiolate or alkynyl ligands. The syntheses, structures and photophysical properties of these heteropolynuclear thiolate/alkynyl complexes are summarized to elucidate the correlation between structures and luminescence.

Keywords: Alkynyl; Coinage metal; Heteropolynuclear; Luminescence; Phosphine; Platinum; Thiolate

1. Introduction

The **10** and **11** group metal ions usually exhibit d^8 or d^{10} electronic configurations. One of the most remarkable features of these d^8 or d^{10} metal complexes is their tendency to form metal–metal contacts whose energy is comparable with that of hydrogen bonds [1]. In combination with various anionic or neutral ligands, these d^8 and d^{10} metal ions can form a wide variety

Abbreviations: aet, 2-aminoethanethiolate; bpy, 2,2′-bipyridine; Brphen, 5-bromophenanthroline; dbbpy, 4,4′-dibutyl-2,2′-bipyridine; dmbpy, 4,4′-dimethyl-2,2′-bipyridine; dppm, bis(diphenylphosphino)methane; edt, 1,2-ethanedithiolate; pdt, 1,3-propanedithiolate; phen, 1,10-phenanthroline; tdt, 3,4-toluenedithiolate.

* Corresponding author. Fax: +86 591 8379 2346.
E-mail address: czn@fjirsm.ac.cn (Z.-N. Chen).

0010-8545/$ – see front matter © 2007 Elsevier B.V. All rights reserved.
doi:10.1016/j.ccr.2007.11.015

of coordination compounds that exhibit intriguing spectroscopic and optoelectronic properties [2–5]. Most remarkably, d^8 and d^{10} metal complexes are frequently luminescent with manifold emissive origins depending on their structural features as well as the nature of the metal ions and the ligands[6–14].

In order to reveal the correlation between structures and emissive properties, numerous mono-, di-, tri- or oligonuclear complexes of d^8 or d^{10} metal ions have been prepared with a wide range of ligands including halides, chalcogenides, thiolates, phosphines, acetylides and *N*-heterocycles [2–14]. Noticeably, the presence of thiolate, acetylide and/or phosphine usually favors formation of ligand-linked metal cluster arrays through metal–metal interactions. The metal–metal contacts usually play a significant role in governing the spectroscopic properties and determining the emission features of these d^8 or d^{10} metal cluster compounds [2–14]. Furthermore, the emission energy, lifetime and quantum efficiency are tunable by modifying the ligands as well as introducing electron-donating or -accepting substituents to the aromatic rings.

There are a few review articles dealing with d^8 or d^{10} homonuclear complexes of thiolates [10–13] or alkynyl ligands [14–19], in which the preparation, reactivity and structures of a wide range of oligonuclear d^8 or d^{10} complexes together with their photophysical properties [10–13,18,19] have been extensively reviewed. In contrast, review articles involving d^8–d^{10} or d^{10}–d^{10} heteropolynuclear complexes are scarce [20–22]. This article focuses on presenting the recent progress in the design of luminescent d^8–d^{10}/d^{10}–d^{10} heteropolynuclear and/or multicomponent complexes by incorporating d^8 or d^{10} metal thiolates/acetylides complexes with d^{10} metal diphosphine components. The synthetic routes, spectroscopic and structural characterization together with photophysical properties of a series of d^8–d^{10}/d^{10}–d^{10} heteropolynuclear and/or multicomponent complexes based on thiolate or alkynyl ligands are summarized herein.

2. d^8–d^{10} heteropolynuclear thiolate complexes

Because of the thiolate bonding diversity, metal thiolate complexes are known to adopt various nuclearities and great structural complexity [10–12]. Of numerous metal thiolate species, those with d^8 metal ions such as Ni^{2+}, Pd^{2+}, Pt^{2+} and Au^{3+} are particularly attractive owing to their intriguing spectroscopic and photophysical properties [10,12,13]. A large number of d^8 or d^{10} homonuclear thiolate species with different nuclearities and diverse structural topology have been prepared and the correlation between structure and emission summarized [10,12,13]. In contrast, studies on the photophysical properties of d^8–d^{10} heteropolynuclear thiolate complexes are quite limited [23], to the best of our knowledge, although a number of such species have been reported in the literature [23–28]. González-Herrero and co-workers [23] recently described the preparation of a series of Pt(Pd)Au or Pt(Pd)Au_2 heteropolynuclear thiolate complexes with (2,7-di-*tert*-butylfluoren-9-ylidene)methanedithiolate. Upon formation of the Pt(Pd)Au or Pt(Pd)Au_2 arrays by introducing $[Au(PCy]^+$ units through Pt(Pd)–S–Au linkages, the low-energy absorption due to $d\pi(Pt/Pd) \rightarrow \pi^*$ (dithiolate/diimine) MLCT or charge transfer to diimine state is obviously blue-shifted because of a decrease in the energy level of the mixed metal/dithiolate HOMOs. Both Pd^{II}–Au^I and Pt^{II}–Au^I heteropolynuclear species are emissive at 77 K originating from a metal-centered ^{3}d–d state for the Pd^{II}–Au^I species whereas from a MLCT (Pt → dithiolate) triplet state or admixture of charge transfer to diimine and diimine intraligand $\pi \rightarrow \pi^*$ triplet states for the Pt^{II}–Au^I complexes.

Our recent studies focused on the preparation of luminescent d^8–d^{10} multicomponent and heteropolynuclear thiolate complexes utilizing d^8 metal thiolates as precursors to incorporate with d^{10} coinage metal diphosphine components. Some mononuclear d^8 metal thiolate species containing Ni^{2+}, Pd^{2+}, Pt^{2+} or Au^{3+} ions were selected for construction of a series of luminescent d^8–d^{10} heteropolynuclear thiolate complexes. These compounds exhibit diversified structural topologies and intriguing photophysical properties. Most of them show intense photoluminescence in both solid state and solutions at ambient temperature.

2.1. d^8–d^{10} heteropolynuclear complexes based on Ni^{II}/Pd^{II} thiolate

In view of the prominent bridging character from the S donors in the thiolates, d^8 metal thiolate complexes $M(aet)_2$ (M = Ni, Pd or Pt) are versatile precursors for the construction of heteropolynuclear arrays [29]. Attempts have been made to access d^8–d^{10} heteropolynuclear thiolate complexes using $M(aet)_2$ as precursors, including reactions with d^{10} metal diphosphine species $[M'_2(\mu\text{-dppm})_2(MeCN)_2]^{2+}$ (M′ = Cu or Ag) induced isolation of thiolato-bridged $Cu_4{}^IM_3{}^{II}$ heteroheptanuclear complexes $[Cu_4M_3(\mu\text{-dppm})_3(\mu_3\text{-aet})_4(\mu\text{-aet})_2]^{4+}$ (M = Ni **1**, Pd **2**) or $Ag_2{}^IM^{II}$ heterotrinuclear complexes $[Ag_2M(\mu\text{-dppm})_2(\mu\text{-aet})_2]^{2+}$ (M = Ni **3**, Pd **4**) [30].

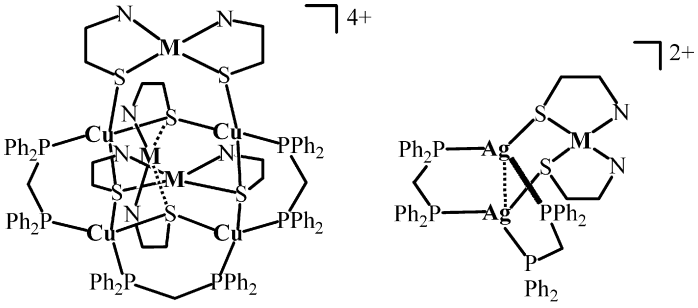

M' = Ni **1**, Pd **2** M' = Ni **3**, Pd **4**

The Cu_4M_3 (M = Ni **1**, Pd **2**) heteroheptanuclear species is probably induced by incorporating three $M(aet)_2$ units with one $[Cu_4(\mu\text{-dppm})_3]^{4+}$ component which is derived from the rearrangement in the original Cu^I component $[Cu_2(\mu\text{-dppm})_2]^{2+}$. The heterotrinuclear Ag_2M (M = Ni **3**, Pd **4**) complexes, however, originate from a direct combination of $M(aet)_2$ with the $[Cu_2(\mu\text{-dppm})_2]^{2+}$ subunit. Formation of the heteroheptanuclear species **1** and **2** for M′ = Cu^I [30] whereas heterotrinuclear complexes 3 and 4 for M′ = Ag^I can be ascribed to the better

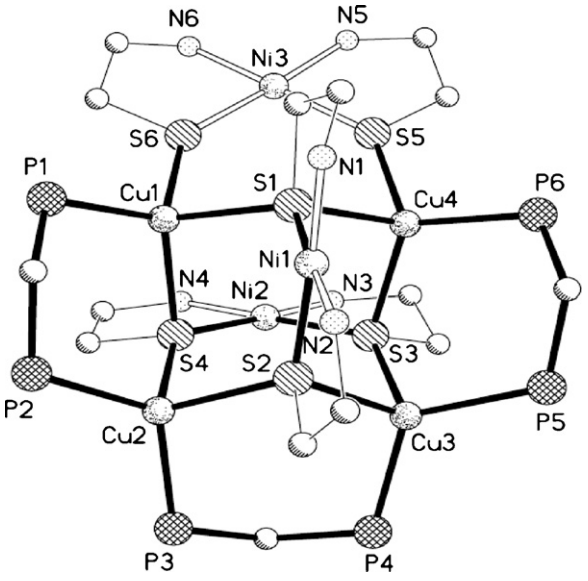

Fig. 1. Perspective view of **1** with atom labeling scheme. The phenyl rings in the phosphorus atoms are omitted for clarity [30].

coordination flexibility of Cu^I than that of Ag^I as well as the absence of Cu^I–Cu^I contacts ($Cu^I\cdots Cu^I > 3.5$ Å) in **1** and **2**, contrasting strikingly to the presence of an argentophilic contact (Ag^I–$Ag^I < 3.0$ Å) in **3** and **4**.

As depicted in Fig. 1, **1** consists of a $Cu_4(\mu\text{-dppm})_3$ unit linked by four μ_3-S donors from two $Ni(aet)_2$ blocks (Ni1 and Ni2) as well as by another two μ-S donors from the third $Ni(aet)_2$ block (Ni3). The Ni^{II}–S–Cu^I and Cu^I–S–Cu^I linkages induce formation of an adamantane-like structure with eight six-membered coordination rings in the Cu_4Ni_3 molecular motif. The coordination planes for Ni1 and Ni2 are almost perpendicular to each other with a dihedral angle of 88.1°. The neighbouring Cu···Cu separations are >3.5 Å, excluding the possibility of a cuprophilic interaction. For the $Ag^I{}_2M^{II}$ (M = Ni or Pd) heterotrinuclear complexes, however, argentophilic contact is obviously operating in view of the short Ag–Ag distance (2.95 Å for **3** and 2.99 Å for **4**). This is probably one of the driving forces for formation of the $NiAg_2$ or $PdAg_2$ heterotrinuclear structure.

The electronic absorption spectra of **1**–**4** in acetonitrile are characterized by absorption shoulders at ca. 270–290 nm with tails extending to *ca*. 400 nm. With excitation at $\lambda_{ex} > 350$ nm, the $Cu_4{}^IM_3{}^{II}$ (M = Ni **1**, Pd **2**) heteroheptanuclear species are room-temperature luminescent at ca. 620 nm with lifetimes in the microsecond range in degassed acetonitrile solutions, originating probably from a spin-forbidden thiolate(S)-to-copper ^{3}LMCT (ligand-to-metal charge transfer) triplet state. The Ag_2M (M = Ni **3**, Pd **4**) complexes, however, show weaker emission compared with that of the $Cu_4{}^IM_3{}^{II}$ species.

2.2. d^8–d^{10} heteropolynuclear complexes based on Au^{III} dithiolate

Like platinum(II), gold(III) adopts a d^8 electronic configuration facile to form an approximately square-planar geometry when chelated by dithiolate ligands. In view of the potentially bridging character and versatile bonding modes of the sulfur donors in $[Au(tdt)_2]^-$ [31], it is a useful precursor for the design of Au^{III}–M^I heterovalent or heteropolynuclear complexes with novel structural topology [32]. As anticipated, incorporation of $[Au(tdt)_2]^-$ with $[M_2(dppm)_2(MeCN)_2]^{2+}$ (M = Cu^I or Ag^I) or $[M_2(dppm)_2]^{2+}$ (M = Au^I) caused isolation of the $Au^{III}Cu_8{}^I$ (**5**), $Au^{III}{}_3Ag^I{}_8$ (**6**) and $Au^{III}Au_4{}^I$ (**7**) complexes when M = Cu^I, Ag^I and Au^I, respectively [32]. The $Au^{III}Au_4{}^I$ product (**7**) is indeed derived from a direct combination of two binuclear $[Au_2{}^I(dppm)_2]^{2+}$ units with one $[Au^{III}(tdt)_2]^-$ block through Au^I–S–Au^{III} linkages. The $Au^{III}Cu_8{}^I$ (**5**) and $Au_3{}^{III}Ag_8{}^I$ (**6**) complexes, however, arise from dissociation and recombination in the original metal components $[Au(tdt)_2]^-$ and $[M_2(dppm)_2(MeCN)_2]^{2+}$ (M = Cu^I or Ag^I).

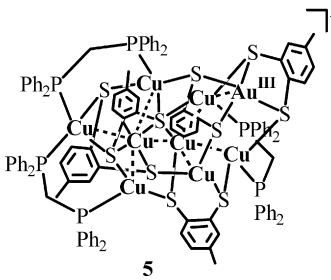

5

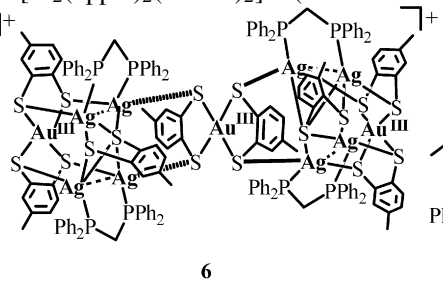

6

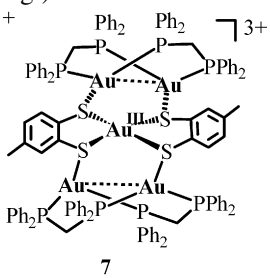

7

As indicated in Scheme 1, three forms of conformations are exhibited in **5**–**7** based on different orientations of the four Au^{III}–S–M linkages in square-planar $Au(tdt)_2$ subunits. While *syn* occurs in **5** ($Au^{III}Cu_8{}^I$) and *anti*-2 in **7** ($Au^{III}Au_4{}^I$), both *syn* and *anti-1* are present in **6** ($Au_3{}^{III}Ag_8{}^I$). Depending on the number and orientation of the Au^{III}–S–M^I or M^I–S–M^I linkages, the tdt ligand exhibits five types of bonding modes as depicted in Scheme 2. Note that the bonding modes I and II only differ in orientation of the Au^{III}–S–M^I linkages so as to display *syn* (mode I) or *anti* (mode II) arranged forms [32]. It is intriguing that the narrower Au^{III}–S–M^I or M^I–S–M^I angles are always correlated with the shorter Au^{III}–M^I or M^I–M^I contacts in **5**–**7**.

The $Au^{III}Cu_8{}^I$ complex **5** (Fig. 2) arises likely from the combination of $[Cu_8{}^I(\mu\text{-dppm})_3(tdt)_3]^{2+}$ with $[Au(tdt)_2]^-$ through four Au^{III}–S–Cu^I linkages in *syn* form, in which formation of the octanuclear Cu_8 component is involved in dissociation and recombination of the original precursors. The tdt ligand adopts bonding modes I, III and IV (Scheme 2) to form the $Au^{III}Cu_8{}^I$ cluster array through both Au^{III}–S–Cu^I and Cu^I–S–Cu^I linkages. The considerable short Cu^I–Cu^I distances (2.70–2.99 Å) indicate significant cuprophilic contacts [1]. The

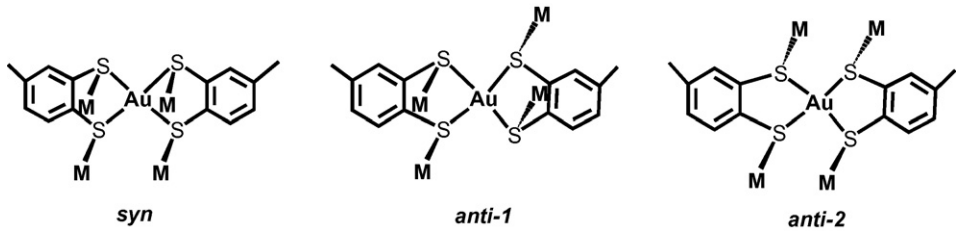

Scheme 1.

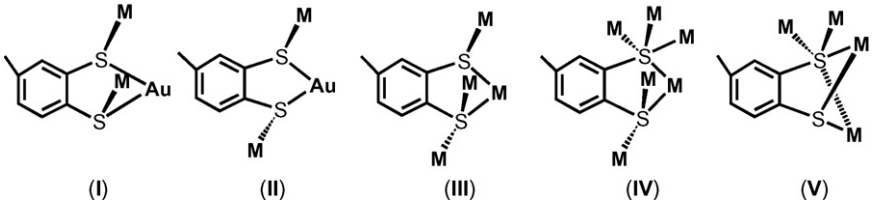

Scheme 2.

shortest intramolecular $Cu^{I}\cdots Au^{III}$ distances (3.216(4) Å and 3.376(4) Å) suggest a weak Cu^{I}–Au^{III} interaction [33]. The $Au_3{}^{III}Ag_8{}^{I}$ complex **6** (Fig. 3) is likely formed by incorporating three $Au(tdt)_2$ units with two $Ag_4(\mu\text{-dppm})_2(tdt)$ fragments through Au^{III}–S–Ag^{I} linkages in two different oriented forms, where the Au^{III}–S–Ag^{I} linkages for the $Au(tdt)_2$ subunit at the middle adopts *anti-1* form (Scheme 1) whereas those at the two sides display the *syn* form. The tdt ligand adopts mode I and V (Scheme 2) to link Au^{III}–Ag^{I} and Ag^{I}–Ag^{I}, respectively. Weak Ag^{I}–Ag^{I} and Au^{III}–Ag^{I} contacts are possibly operating [34] in view of the Ag^{I}–Ag^{I} (3.26–3.32 Å) and the shortest Au^{III}–Ag^{I} (ca. 3.51 Å) distances. The $Au^{III}Au_4{}^{I}$ complex **7** consists of one $[Au(tdt)_2]^{-}$ associated with two $[Au_2(\mu\text{-dppm})_2]^{2+}$ units through Au^{III}–S–Au^{I} linkages in *anti-2* (Scheme 1) form. The tdt ligand adopts an *anti*-oriented mode II (Scheme II) to form the Au^{III}–S–Au^{I} linkages. The Au^{I}–Au^{I} (3.1253(13) Å and 3.1668(9) Å) distances imply the presence of aurophilicity [5]. The Au^{I}–Au^{III} (3.43–4.18 Å) contact, however, is negligible.

In contrary to non-emissive $Au^{III}Cu_8{}^{I}$ (**5**) and $Au^{III}{}_3Ag_8{}^{I}$ (**6**) species, $Au^{III}Au_4{}^{I}$ (**7**) complex luminesces strongly in both the solid state and fluid acetonitrile with microsecond lifetimes at room temperature. Since the $Au^{III}(tdt)_2$ chromophore is non-emissive, the luminescence in **7** is most likely induced by the $Au_2(\mu\text{-dppm})_2$ chromophore and/or the Au^{III}–S–Au^{I} linkages. The emission (λ_{em} = 570 nm) is obviously blue-shifted compared with that of the precursor $[Au(dppm)]_2(BF_4)_2$ (λ_{em} = 593 nm, $Au^{I}\cdots Au^{I}$ = 2.93 Å) [35] due to the significantly elongated Au^{I}–Au^{I} distance in **7** (ca. 3.15 Å).

Electrochemical studies indicate that reversible redox waves occur at 0.16 and −1.08 V for **5** in dichloromethane solution of 0.10 M $(Bu_4{}^{n}N)(PF_6)$, due to probably one-electron oxidation of tdt and metal-centered one-electron reduction, respectively. The significant positive shift of the metal-centered reduction in **5** relative to that of the parent compound $[Bu_4N][Au(tdt)_2]$ [36] is a direct consequence of the formation of the $Au^{III}Cu_8{}^{I}$ cluster structure. On the contrary, irreversible ligand oxidation and metal-centered reduction waves occur in both **6** and **7** due

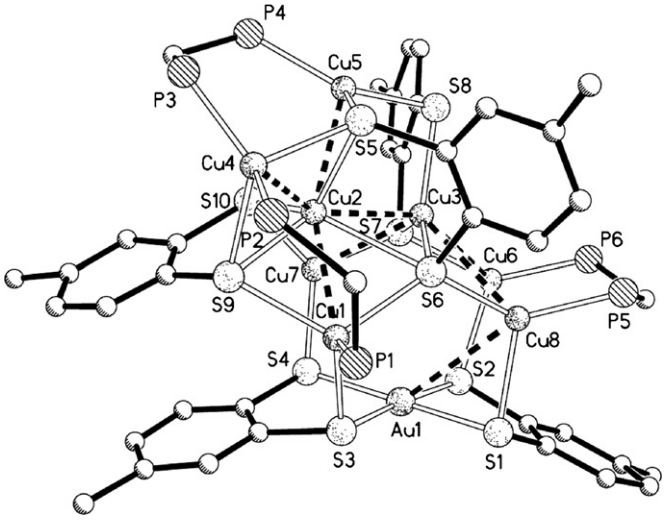

Fig. 2. Perspective view of **5** with atom labeling scheme. The phenyl rings in the phosphorus atoms are omitted for clarity [32].

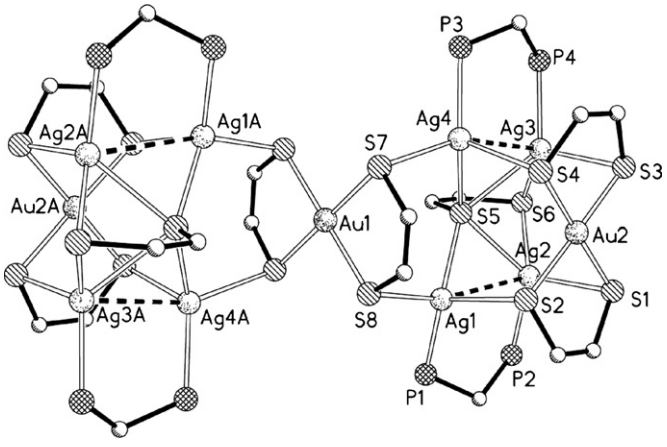

Fig. 3. Perspective view of **6** with atom labeling scheme. The phenyl rings in the phosphorus atoms are omitted for clarity [32].

probably to sample dissociation during electrochemical measurements.

2.3. d^8–d^{10} heteropolynuclear complexes based on Pt(dithiolate)(diimine)

Mononuclear platinum(II) diimine dithiolate complexes usually exhibit long-lived photoluminescence with readily tunable emission energy when electron-donating or -accepting substituents are introduced to the diimine and/or dithiolate ligands [10,37,38]. In view of the potential bridging character of the S donors in the dithiolates, Pt(diimine)(dithiolate) complexes can serve as excellent precursors for the design of multicomponent or heteropolynuclear complexes that emit efficient and long-lived photoluminescence with a wide range of emissions or colors [39,40]. As anticipated, incorporation of Pt(diimine)(dithiolate) with d^{10} coinage metal diphosphine components including $M_2(dppm)_2(MeCN)_2^{2+}$ (M = Cu, Ag) and $Au_2(dppm)_2^{2+}$ affords a feasible approach to access luminescent Pt^{II}–M^{I} (M = Cu, Ag, Au) heteropolynuclear complexes. Nevertheless, only in a few cases do the Pt^{II}–M^{I} heteropolynuclear products result from direct combination of Pt(diimine)(dithiolate) with $M_2(dppm)_2(MeCN)_2^{2+}$ or $Au_2(dppm)_2^{2+}$, while in most cases the isolated products are derived not only from dissociation and recombination of the metal starting components, but also from disruption of the C–S bonds in the dithiolates [39,40]. Rearrangement of Pt(diimine)(dithiolate) and $[Cu_2(dppm)_2]^{2+}$ components during the reaction is likely correlated with various factors including the different affinities of Pt^{II} and Cu^{I} for the S, P and N donors, steric requirement, and thermodynamic stability, etc.

2.3.1. Pt^{II}–Cu^{I} heteropolynuclear dithiolate complexes

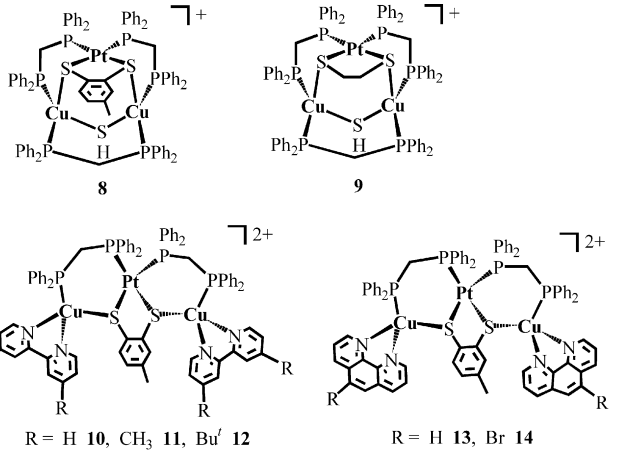

8 **9**

R = H **10**, CH_3 **11**, Bu^t **12** R = H **13**, Br **14**

R = H **15**, Bu^t **16** R = H **17**, Br **18**

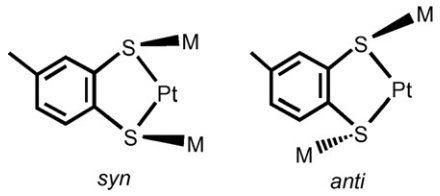

syn *anti*

Scheme 3.

Reactions of Pt(diimine)(tdt) with $Cu_2(dppm)_2(MeCN)_2^{2+}$ led to the isolation of the unexpected $Pt^{II}Cu^{I}_2$ heterotrinuclear complexes $[PtCu_2(tdt)(\mu\text{-}SH)(dppm)_3]^+$ (**8**) together with $[PtCu_2(diimine)_2(tdt)(dppm)_2]^{2+}$ (diimine = bpy **10**, dmbpy **11**, dbbpy **12**, phen **13**, Brphen **14**) [39]. When edt is used in place of tdt [40], heterotrinuclear complexes $[PtCu_2(edt)(\mu\text{-}SH)(dppm)_3]^+$ (**9**) and $[PtCu_2(diimine)_2(edt)(dppm)_2]^{2+}$ (diimine = bpy **15**, dbbpy **16**, phen **17**, Brphen **18**) were isolated.

In these $Pt^{II}Cu_2^{I}$ arrays, the dithiolate exhibits a chelating and bridging coordination mode, resulting in a heterotrinuclear assembly with the Pt–S–Cu linkages in *syn* or *anti* form [39] as depicted in Scheme 3. While the *syn* form occurs in $Pt_2^{II}Cu^{I}$ dithiolate species **8** (Fig. 4) and **9**, the *anti* form is observed in $Pt^{II}Cu_2^{I}$ dithiolate diimine complexes **10**–**18** (Fig. 5). In both oriented forms, the least-square plane built by S_2P_2 (for **8** and **9**) or S_2N_2 (for **10**–**18**) donors is almost perpendicular to that formed by S_2Cu_2 atoms. The chelating Pt–S lengths are usually shorter than the bridging Cu–S distance in the Pt–S–Cu arrays. The dppm acts as a bridging ligand to link both $Pt^{II}\cdots Cu^{I}$and $Cu^{I}\cdots Cu^{I}$ centers. The considerably long $Pt^{II}\cdots Cu^{I}$ (>3.2 Å) and $Cu^{I}\cdots Cu^{I}$ (>3.2 Å) distances suggest the intermetallic contacts are weak or absent.

The UV–vis absorption spectra of $Pt_2^{II}Cu^{I}$ complexes **8**–**18** in acetonitrile solutions (Table 1) are characterized by intense high-energy absorption at ca. 230–260 nm with a shoulder at ca. 280–300 nm in addition to low-energy shoulders at 355–420 nm. They are non-emissive in fluid solutions, but show room-temperature luminescence in the solid state with a lifetimes in the microsecond range (Table 1). They are also luminescent at

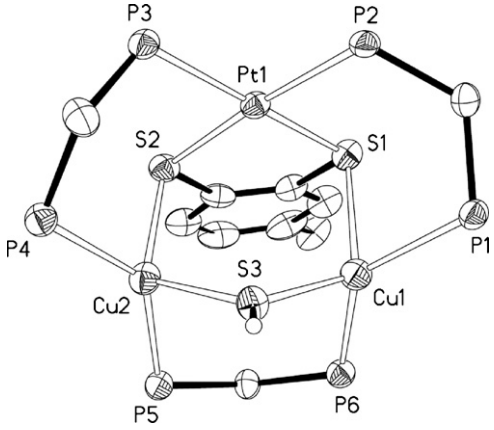

Fig. 4. ORTEP drawing of **8** (30% thermal ellipsoids), showing two *syn*-oriented Pt–S–Cu linkages. Phenyl rings on the phosphorus atoms are omitted for clarity [39].

Table 1
Photophysical data for $PtCu_2$ heterotrinuclear complexes **8–18**

Complexes	Medium	λ_{abs} (nm) (ε, $dm^3\ mol^{-1}\ cm^{-1}$)	λ_{em} (nm) (τ_{em}, μs) at 298 K	λ_{em} (nm) at 77 K
8	Solid		597 (3.27)	585
	MeCN	277 (28,100), 320 (6260)		580
9	Solid			614
	MeCN	268 (41,760), 290 (27,640), 330 (8380)	616 (1.67)	588
10	Solid			615
	MeCN	235 (59,300), 285 (32,640), 360 (5240)	607 (0.22)	583
11	Solid			601
	MeCN	231 (62,820), 292 (26,660), 351 (5410)	593 (0.34)	575
12	Solid			597
	MeCN	220 (64,430), 283 (28,310), 350 (4630)	585 (0.36)	570
13	Solid			599
	MeCN	241 (77,900), 291 (40,740), 408 (5260)	591 (0.56)	576
14	Solid			616
	MeCN	247 (67,400), 288 (46,550), 415 (4700)	606 (0.47)	587
15	Solid			637
	MeCN	225 (76,220), 275 (45,690), 370 (3250)	618 (0.078)	606
16	Solid			614
	MeCN	223 (64,400), 273 (38,780), 375 (4080)	600 (0.21)	600
17	Solid			619
	MeCN	238 (62,660), 268 (61,430), 383 (9760)	601 (0.10)	624
18	Solid			639
	MeCN	245 (57,050), 263 (54,650), 402 (8300)	626 (0.26)	635

77 K both in the solid state and frozen solutions. In view of the distinctly red-shifted emission for the edt complex **9** compared with that for the tdt species **8**, their emissive origin is ascribed to a spin-forbidden dithiolate-to-platinum ^{3}LMCT (ligand-to-metal charge transfer) triplet state, which accords with the electron-donating ability as well as the energy level of the dithiolate ligand with edt > tdt. For the $Pt^{II}Cu_2{}^{I}$ dithiolate diimine species **10–18**, the emission energy depends on the substituents in both diimine and dithiolate ligands. Introducing an electron-donating substituent to the diimine induces a blue shift whereas a red shift occurs for the electron-withdrawing substituent. For the $Pt^{II}Cu_2{}^{I}$ dithiolate diimine complexes containing the same diimine but different dithiolate, the emission of the edt species is always red-shifted relative to that of the corresponding tdt complexes. Consequently, the luminescence in the $Pt^{II}Cu_2{}^{I}$ heterotrinuclear complexes **10–18** originates most likely from an admixture of ^{3}[d(Cu)/p(dithiolate) → π*(diimine)] ^{3}MLCT/LLCT states.

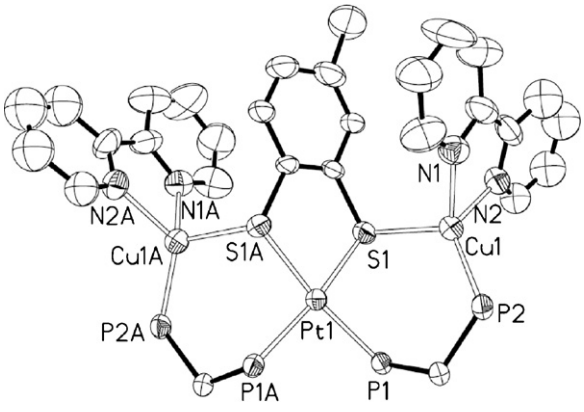

Fig. 5. ORTEP drawing of **10** (30% thermal ellipsoids), showing two *anti*-oriented Pt–S–Cu linkages. Phenyl rings on the phosphorus atoms are omitted for clarity [39].

2.3.2. Pt^{II}–Ag^{I} heteropolynuclear dithiolate complexes

The isolated products by reaction of Pt(diimine)(dithiolate) with $Ag_2(dppm)_2(MeCN)_2{}^{2+}$ are dependent on the nature of the dithiolate ligands. When dithiolate = tdt, the major products are the desired heterotrinuclear complexes $[PtAg_2(diimine)(tdt)(dppm)_2]^{2+}$ (diimine = bpy **20**, dmbpy **21**,phen **22**, Brphen **23**) together with an unexpected complex $[PtAg_2(tdt)(\mu\text{-}SH)(dppm)_3]^{+}$ (**19**) as a minor species [39]. When dithiolate = edt or pdt, nevertheless, an unexpected colorless $Pt_2{}^{II}Ag_2{}^{I}$ heterotetranuclear species

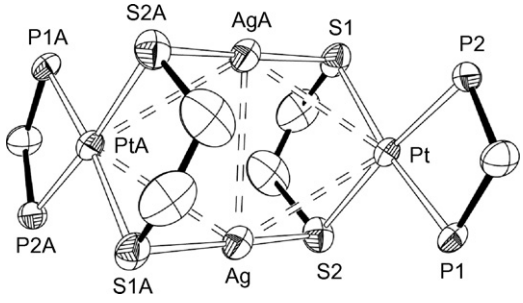

Fig. 6. ORTEP drawing of **24** (30% thermal ellipsoids). Phenyl rings on the phosphorus atoms are omitted for clarity [40].

$[Pt_2Ag_2(dithiolate)_2(dppm)_2]^{2+}$ (dithiolate = edt **24**, pdt **25**) is the only species isolated [40].

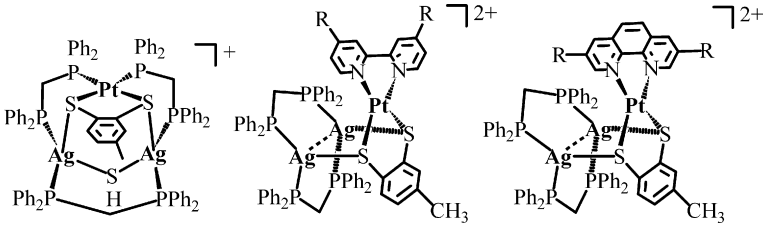

19 R = H **20**, CH_3 **21** R = H **22**, Br **23**

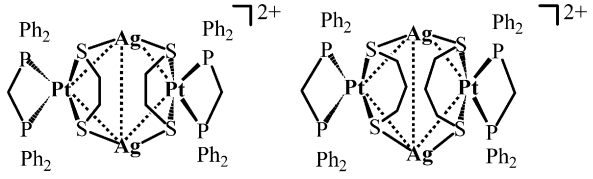

24 **25**

The $PtAg_2$ dithiolate species **19** with Ag^I in place of Cu^I corresponds to the counterpart of $PtCu_2$ species **9**. The $PtAg_2$ dithiolate diimine complexes **20**–**23** is composed of a $Ag_2(dppm)_2$ unit associated with Pt(diimine)(tdt) through the Pt–S–Ag linkages in *syn* form (Scheme 3). The Pt^{II} coordination plane with N_2S_2 donors are almost perpendicular to the plane composed of Ag_2S_2 atoms. The Ag^I–Ag^I distances (2.90–3.10 Å) imply a moderate argentophilicity [1]. The Pt^{II}–Ag^I distances are in the range of 3.20–3.50 Å, suggesting weak intermetallic contacts. The Pt_2Ag_2 species **24** and **25** consist of two Pt(dppm)(dithiolate) (dithiolate = edt **24**, pdt **25**) units incorporating with two Ag^I atoms through Pt–S–Cu linkages in *syn* form (Fig. 6), giving a distorted rhombic Pt_2Ag_2 cluster. The Ag–Pt distances (3.06–3.15 Å) are slightly shorter than those (3.24–3.43 Å) in $Pt_2^{II}Ag_2^I$ heterotetranuclear 1,1-ethylenedithiolato complexes $[Pt_2Ag_2(PPh_3)_2\{S_2C{=}C\{C(O)Me\}_2\}_2](ClO_4)_2$ containing PPh_3 [28]. The Ag–Ag distances (ca. 3.27 Å), however, are longer than those (3.14 Å) in the $Pt_2^{II}Ag_2^I$ 1,1-ethylenedithiolato complexes [28]. The intramolecular Pt···Pt distances (5.27 Å for **24** and 5.34 Å for **25**) are far beyond the distances for intermetallic interactions. The Ag^I atoms are located up the Pt^{II} coordination planes 2.33 Å for **24** and 2.40 Å for **25**. In contrast to the bridging character of the dppm ligand in **8**–**23**, the Pt^{II} center is chelated by η^2-dppm in the Pt_2Ag_2 species.

Table 2
Photophysical data for Pt^{II}–M^I (M = Ag, Au) heteropolynuclear thiolate complexes **19**–**28**

Complexes	Medium	λ_{abs} (nm) (ε, $dm^3\ mol^{-1}\ cm^{-1}$)	λ_{em} (nm) (τ_{em}, μs) at 298 K	λ_{em} (nm) at 77 K
19	Solid		605 (2.85)	574
	MeCN	275 (32,830), 319 (6110), 347 (4350)		574
20	Solid		593 (4.72)	598
	MeCN	230 (59,400), 304 (16,060), 328 (6080), 469 (2560), 555 (2120)	673	602
21	Solid		571 (2.56)	575
	MeCN	224 (66,670), 290 (26,820), 325 (7650), 450 (3480), 540 (980)	645	575
22	Solid		577 (0.84)	589
	MeCN	243 (91,410), 268 (59,140), 312 (10,450), 458 (4670), 550 (2690)	688	635
23	Solid		608 (3.65)	613
	MeCN	240 (67,470), 275 (49,780), 318 (6810), 469 (2240), 565 (1380)	700	647
24	Solid			648
	MeCN	222 (63,800), 245 (64,980), 320 (5042)		605
25	Solid			664
	MeCN	229 (52,590), 246 (54,340), 330 (5130)		614
26	Solid		642 (1.44)	631
	MeCN	242 (67,200), 293 (55,900), 549 (7020)	606 (0.035)	660
27	Solid		609 (1.17)	605
	MeCN	226 (61,780), 294 (43,000), 533 (4320)	576 (0.021)	629
28	Solid		563 (0.66)	625
	MeCN	221 (68,500), 240 (70,180), 320 (5570)	556 (0.015)	598

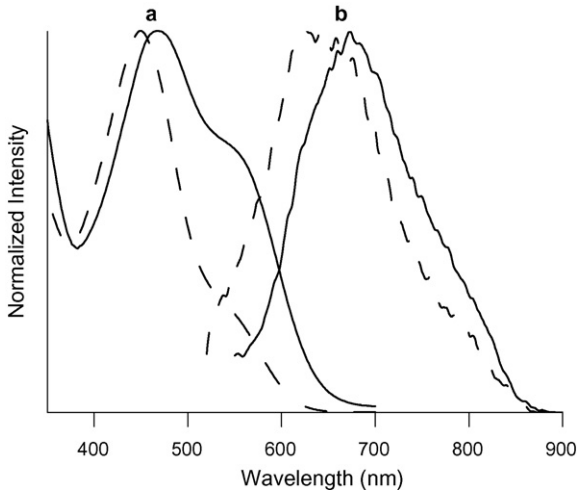

Fig. 7. Absorption (a) and emission (b) spectra of **20** (solid) and **21** (dash) in MeCN at 298 K [39].

In addition to intense ligand-centered absorption in the UV region, $PtAg_2$ heterotrinuclear dithiolate diimine complexes **20–23** (Table 2) in acetonitrile solutions display broad absorption bands at ca. 450–470 nm with a shoulder at ca. 540–565 nm. This low-energy absorption arising probably from charge transfer to the diimine [37,38] is dependent on the substituents in the diimine ligands. By comparison of the low-energy absorption bands of **20** with **21** and those of **22** with **23**, a blue shift from **20** to **21** (Fig. 7) whereas a red shift from **22** to **23** occurs.

By irradiation of **20–23** at λ_{ex} = 350–550 nm, a region where there occur states due to charge transfer to the diimine, these $PtAg_2$ complexes show room-temperature luminescence in both the solid state and fluid acetonitrile solution (Fig. 7) with the lifetimes in the microsecond range (Table 2). These arise most likely from ^{3}[d(Pt)/p(dithiolate) → π*(diimine)] MLCT/LLCT triplet states as described in the corresponding precursors Pt(diimine)(tdt) [37,38]. The emission energies, however, are noticeably blue-shifted (ΔE_{em} = 0.10–0.35 eV) upon formation of $PtAg_2$ heterotrinuclear complexes **20–23** owing to incorporating the Pt(diimine)(tdt) with $[Ag_2(dppm)_2]^{2+}$ subunits, thus raising the emissive energy of the square planar Pt(diimine)(dithiolate) chromophores. The Pt_2Ag_2 heterotetranuclear species **24** and **25** (Table 2) are only emissive at 77 K. The excited state is ascribed as a [dithiolate → Pt_2Ag_2] LMCT transition, modified by Pt–Ag and Ag–Ag contacts [41]. Because of the better electron-donating capability of pdt than that of edt, the emission of the pdt complex **25** is slightly red-shifted relative to that of the edt complex **24** both in the solid state and in frozen acetonitrile at 77 K.

2.3.3. Pt^{II}–Au^{I} heteropolynuclear dithiolate complexes

Reactions of Pt(diimine)(dithiolate) with $[Au_2(dppm)_2]^{2+}$ caused isolation of the desired complexes $[PtAu_2(diimine)(tdt)(dppm)_2]^{2+}$ (diimine = bpy **26**, dmbpy **27**) when dithiolate = tdt [40], but an unexpected complex $[PtAu_2(edt)(dppm)_2]^{2+}$ (**28**) was isolated when dithiolate = edt [40]. The ^{31}P NMR spectrum of **26** (36.8 ppm) and **27** (35.9 ppm) exhibits only one singlet since the P donors are only bonded to the Au^{I} atoms instead of the Pt^{II} center. For **28**, typical Pt–P coupling satellite peaks occur at −49.4 ppm with J_{Pt-P} = 1264 Hz in addition to one singlet at 33.2 ppm due to the P donors bound to Au^{I} centers. The dppm chelates the Pt^{II} or bridges the Au^{I} centers in symmetric mode so that the two P donors in each dppm are equivalent.

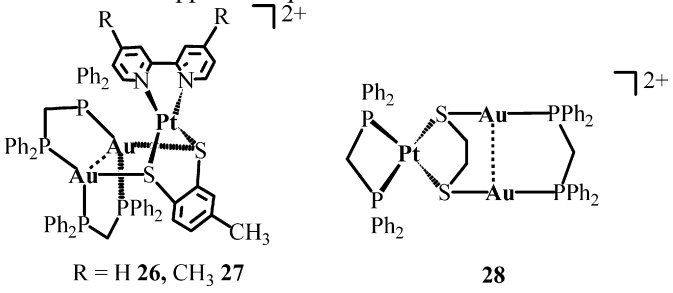

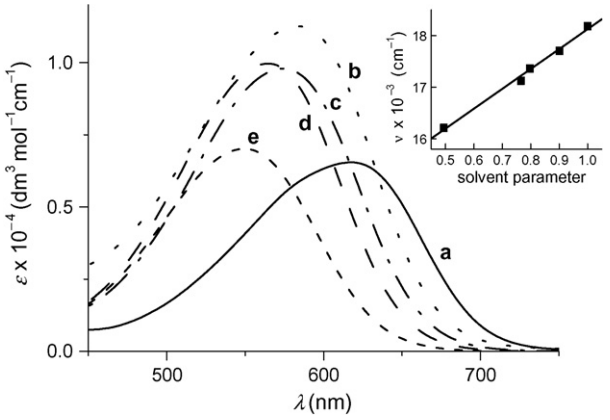

Fig. 8. Charge-transfer-to-diimine absorption band of **26** in THF (a), CH_2Cl_2 (b), acetone (c), DMF (d) and CH_3CN (e) [40]. (Inset) A plot of the energy of the lowest absorption band of **26** as a function of solvent parameter.

The UV–vis spectra of **26** and **27** (Table 2) are characterized by ligand-centered absorptions at ca. 230–240 nm and 290 nm as well as a broad and solvent-dependent low-energy absorption in the visible region, arising likely from [d(Pt)/p(dithiolate) → π*(diimine)] MLCT/LLCT transitions [37,38]. As indicated in Fig. 8, the low-energy absorption exhibits a negative solvatochromism in which it is significantly red-shifted with decrease of solvent polarity, in agreement with the supposition that a charge transfer process occurs indeed from an orbital of a mixed metal/dithiolate character to a diimine π* orbital [42,43]. The UV–vis spectrum of $PtAu_2$ species **28** exhibits ligand-centered bands at 220 and 240 nm together with absorption at ca. 320 nm extending to 400 nm probably due to a [d(Pt/Au) → π(dithiolate)] MLCT state.

26 and **27** show intense room-temperature luminescence in both the solid state and degassed acetonitrile with lifetimes in the microsecond range (Table 2), resulting from ^{3}[d(Pt)/p(dithiolate)→ π*(diimine)] MLCT/LLCT triplet state. Noticeably, the emission of $Pt^{II}Au_2{}^{I}$ species **26** and **27** both in the solid state and fluid solutions is notably blue-shifted (ΔE_{em} = 0.17–0.35 eV) relative to that of the corresponding precursor Pt(diimine)(tdt) [37,38] as observed in $Pt^{II}Ag_2{}^{I}$ complexes **20–23**. Consequently, a wider range of emission or

colors has been achieved for the square planar Pt^{II} diimine chromophores with tunable emission energy by incorporating the metal components $[M_2(dppm)_2]^{2+}$ (M = Au or Ag) so as to alter the energy gap between the HOMO and LUMO. With excitation at $\lambda_{ex} > 300$ nm, **28** displays room-temperature luminescence in both the solid state and fluid acetonitrile solution with sub-microsecond lifetimes, induced perhaps by the dithiolate-to-metal cluster ^{3}[dithiolate → $PtAu_2$] LMCT triplet state.

3. d^8–d^{10}/d^{10}–d^{10} heteropolynuclear alkynyl complexes

By analogy with the d^8/d^{10} metal thiolate compounds, group **10** or **11** metal alkynyl complexes of d^8 or d^{10} ions always display intriguing luminescence with manifold emissive origins [14,18,19]. Diversity in group **10** or **11** metal alkynyl chemistry is also enhanced owing to facile formation of metallophilic interactions between the d^8/d^{10} metal ions [14–19]. Nevertheless, compared with numerous homonuclear alkynyl complexes with d^8 or d^{10} metal ions [14–19], the chemistry of d^8–d^{10} [20] or d^{10}–d^{10} [21] heteropolynuclear alkynyl complexes is in its infancy because of difficulty in controlling the heterometallic arrays. Taking advantage of the potentially bridging C donors in simple σ-bonding metal acetylides, one of the possible synthetic strategies for attaining d^8–d^{10} or d^{10}–d^{10} heteropolynuclear alkynyl arrays is to incorporate d^8 or d^{10} metal acetylides with d^{10} coinage metal components.

3.1. d^8–d^{10} heteropolynuclear alkynyl complexes based on $[Pt(C{\equiv}CR)_4]^{2-}$

Although a number of d^8–d^{10} heteropolynuclear alkynyl complexes [44–47] have been prepared by incorporating d^8 metal alkynyl complexes with d^{10} metal components or by reaction of d^8 metal units with polymeric d^{10} metal acetylides $[M(C{\equiv}CR)]_n$, studies on their luminescent properties are limited [48–54]. Yam et al. prepared a series of PtM_2 and Pt_2M_2 ($M = Cu^I$ or Ag^I) alkynyl complexes [20,55–57] through encapsulation of Cu^+ or Ag^+ ion between two acetylides in the face-to-face diplatinum(II) species $[Pt(\mu\text{-}dppm)_2(C{\equiv}CPh)_4]$ or mononuclear complex Pt^{II} $[Pt(dppy)(C{\equiv}CPh)_2]$ (dppy = 2-diphenylphosphinopyridine) via π-coordination. Encapsulation of copper(I) or silver(I) metal ions in the heterotri- or tetranuclear complexes induced obviously red-shifted MMLCT absorption and ^{3}MMLCT emission compared to that of the face-to-face diplatinum(II) or mononuclear Pt^{II} precursor. Forniés and Lalinde et al. reported the preparation of a series of heterotrinuclear ($PtCu_2$ or $PtAg_2$) and heterohexanuclear (Pt_2Cu_4 or Pt_2Ag_4) alkynyl complexes [49,58] using the Pt^{II} complex to depolymerize the polymeric metal acetylides $[Cu(C{\equiv}CR)]_n$/$[Ag(C{\equiv}CR)]_n$ [58] or from direct reaction of Pt^{II} acetylide components with the d^{10} coinage metal ion [49]. By comparison of the emission spectra of a series of related complexes, the emitting states were ascribed as a substantial cluster $[PtM_2]$/$[Pt_2M_4]$-to-ligand (C≡CR) character (CLCT).

Among a number of available d^8 metal alkynyl precursor species, the tetra-alkynylplatinate(II) complexes $[Pt(C{\equiv}CR)_4]^{2-}$ are particularly useful for the construction of heterometallic alkynyl cluster complexes because of their potentially bridging character in the four alkynyl ligands through σ or/and π coordination [50]. A family of Pt–Cu [52–54], Pt–Ag [50,51,53], Pt–Tl [59,60], and Pt–Cd [61], heteropolynuclear cluster complexes with $[Pt(C{\equiv}CR)_4]^{2-}$ as building blocks have been synthesized. They exhibit remarkable photophysical properties associated with the metal–metal and η^2-M bonding interactions. Particularly, a series of d^8–d^{10} Pt_2M_4 (M = Cu, Ag) heterohexanuclear alkynyl complexes $[Pt_2M_4(C{\equiv}CR)_8]$ (R = Bu^t or Ph) were obtained by Forniés and Lalinde et al. [50] from the reactions of $[PtCl_2(tht)_2]$ (tht = tetrahydrothiophene) with polymeric silver acetylides $[Ag(C{\equiv}CR)]_n$. Crystallization in different solutions and concentrations induced isolation of solid samples of the dimers $[Pt_2M_4(C{\equiv}CR)_8]_2$ [50] and trimers $[Pt_2M_4(C{\equiv}CR)_8]_3$ [52], where the discrete dimers or trimers of the Pt_2M_4 heterohexanuclear octahedral cluster units are stabilized by ligand-unsupported intercluster Pt–Pt interactions. The dimeric species $[Pt_2M_4(C{\equiv}CPh)_8]_2$ were also isolated by Yam et al. [53,54] from direct reaction of the tetra-alkynylplatinate(II) complexes $[Pt(C{\equiv}CPh)_4]^{2-}$ with $[M(MeCN)_4]^+$ ($M = Cu^+$, Ag^+). It is intriguing that with the monomeric Pt_2M_4 hexanuclear octahedral cluster species aggregating into dimers and trimers through ligand-unsupported intercluster Pt–Pt contacts, the luminescence is significantly red-shifted from near-visible (monomers) to near-infrared region (trimers) [52].

We have been interested in the design of Pt–M (M = Cu, Ag, Au) heteropolynuclear alkynyl arrays by incorporating the tetra-alkynylplatinate(II) complexes $[Pt(C{\equiv}CR)_4]^{2-}$ with d^{10} coinage metal diphosphine components in order to explore the luminescent properties of d^8–d^{10} heterometallic alkynyl species and to

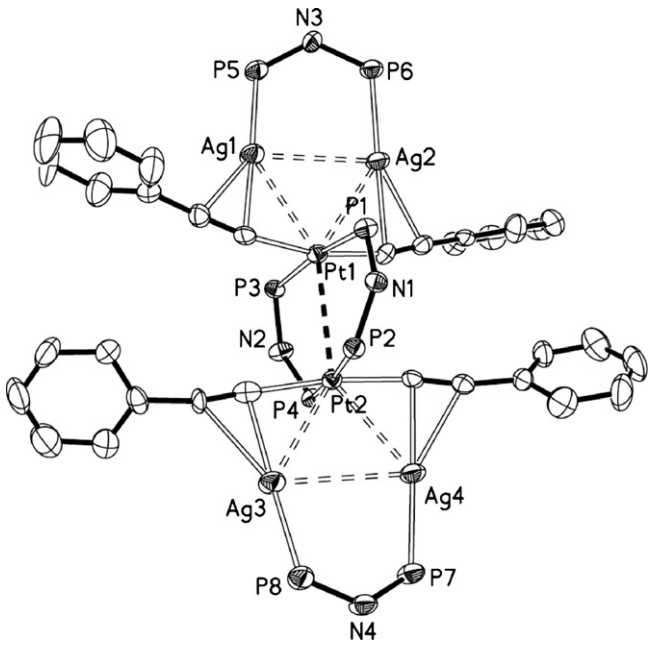

Fig. 9. OPTEP drawing of **29** (30% thermal ellipsoids) with atom labeling scheme [63].

develop their potential applications as optoelectronic materials at the molecular level.

3.1.1. Pt^{II}–Ag^{I} alkynyl complexes based on $[Ag_2(\mu\text{-}PPh_2NHPPh_2)_2]^{2+}$

Reaction of $[Pt(C{\equiv}CC_6H_4R\text{-}p)_4]^{2-}$ (R = H, CH_3) with $[Ag_2(\mu\text{-}PPh_2NHPPh_2)_2(MeCN)_2]^{2+}$ induced isolation of neutral heterohexanuclear complexes $Pt_2Ag_4(\mu\text{-}Ph_2PNPPh_2)_4(C{\equiv}CC_6H_4R\text{-}p)_4$ (R = H **29**, CH_3 **30**) [62]. Instead of resulting from a direct incorporation of the metal component $[Pt(C{\equiv}CC_6H_4R\text{-}p)_4]^{2-}$ (R = H, CH_3) with $[Ag_2(\mu\text{-}PPh_2NHPPh_2)_2(MeCN)_2]^{2+}$, they are better described as the combination of one anionic component $[Pt_2(\mu\text{-}Ph_2PNPPh_2)_2(C{\equiv}CC_6H_4R\text{-}p)_4]^{2-}$ (R = H **1**, CH_3 **2**) with two cationic fragments $[Ag_2(\mu\text{-}Ph_2PNPPh_2)]^{+}$. It is likely that formation of the neutral Pt_2Ag_4 heterohexanuclear clusters is a direct consequence of the facile deprotonating character of PPh_2NHPPh_2.

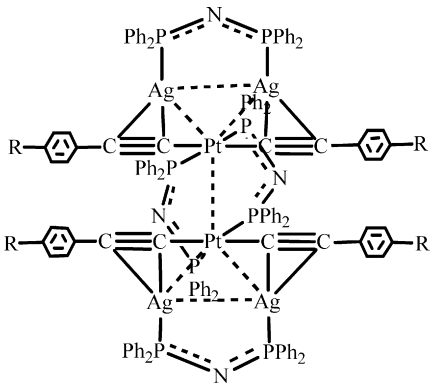

As depicted in Fig. 9, the neutral Pt_2Ag_4 array consists of anionic moiety $[Pt_2(\mu\text{-}Ph_2PNPPh_2)_2(C{\equiv}CC_6H_4R\text{-}p)_4]^{2-}$ and two cationic units $[Ag_2(\mu\text{-}Ph_2PNPPh_2)]^{+}$, in which the anionic diplatinum(II) component adopts a face-to-face arrangement with the two square-planar Pt^{II} coordination planes oriented in parallel fashion [62]. The Pt^{II} atom is surrounded by two

Table 3
Photophysical data for Pt^{II}–M^{I} (M = Cu, Ag, Au) heteropolynuclear alkynyl complexes **31**–**43**

Complexes	Medium	λ_{abs} (nm) (ε, $dm^3\ mol^{-1}\ cm^{-1}$)	λ_{em} (nm) (τ_{em}, μs) at 298 K	λ_{em} (nm) at 77 K
29	Solid		712 (7.2)	
	CH_2Cl_2	401 (10,970), 487 (19,140)	705 (7.4)	
	MeCN	346 (50,000), 485 (23,930)	711 (8.7)	
30	Solid		704 (9.2)	
	CH_2Cl_2	401 (9390), 485 (10,340)	698 (11.4)	
	MeCN	350 (64,460), 484 (17,640)	682 (12.1)	
31	Solid		481 (3.5)	472, 517 (sh)
	CH_2Cl_2	248 (37,920), 270 (35,830), 318 (17,210), 376 (16,850)	428 (3.1 ns), 544 (2.9)	463
32	Solid		495 (1.5)	495
	CH_2Cl_2	256 (39,180), 271 (36,910), 314 (15,940), 383 (16,640)	434 (2.9 ns), 543 (2.8)	473
33	Solid		512 (0.8)	514
	CH_2Cl_2	256 (36,290), 271 (32,720), 394 (15,960)	442 (12.3 ns), 540 (0.06)	485
34	Solid		558 (7.1)	569
	CH_2Cl_2	241 (41,440), 314 (16,190), 364 (6610)	412 (10.3 ns)	485
35	Solid		492 (2.0)	481
	CH_2Cl_2	243 (39,760), 262 (35,410), 354 (12,880), 383 (13,730)	422 (6.7 ns)	475
36	Solid		496 (3.2)	485
	CH_2Cl_2	238 (37,350), 357 (7890), 391 (9460)	434 (6.7 ns)	476
37	Solid		495 (5.2)	489, 538 (sh)
	CH_2Cl_2	264 (42,000), 281 (35,040), 360 (11,540), 403 (16,980)	449 (8.1 ns)	495
38	Solid		509 (6.1)	514
	CH_2Cl_2	242 (32,700), 276 (15,000), 341 (9750)	415 (11.1 ns)	496
39	Solid		484 (0.9)	474, 521 (sh)
	CH_2Cl_2	246 (38,640), 329 (15,070), 393 (10,350)	455 (0.5)	469
40	Solid		579 (6.7)	574
	CH_2Cl_2	312 (20,800), 376 (18,890)	528 (8.8), 420 (3.6 ns)	549, 493 (sh)
41	Solid		500 (1.2), 600	485
	CH_2Cl_2	256 (40,260), 280 (34,330), 351 (17,940), 382 (16,530)	497 (4.1)	474
42	Solid		604 (3.6)	555
	CH_2Cl_2	239 (47,580), 335 (8940)	621 (5.7)	512
43	Solid		576 (1.7, 0.3)	567
	CH_2Cl_2	232 (145,640), 261 (33,940), 380 (39,060)	437 (3.2 ns)	543

trans-arranged acetylide C atoms through $\eta^1(\sigma)$ bonding and two *trans*-oriented P donors from the deprotonated Ph_2PNPPh_2. The Pt–Pt distances (3.15 Å for **29** and 3.11 Å for **30**) are much shorter than those found in face-to-face diplatinum(II) complexes $Pt_2(\mu\text{-}Ph_2PCH_2PPh_2)_2(C{\equiv}CC_6H_4R\text{-}p)_4$ (3.25–3.44 Å) [55,56], implying the presence of stronger intermetallic contacts. The shortening of the Pt–Pt distance is likely a direct consequence because of incorporating the $[Ag_2(PPh_2PNPPh_2)]^+$ moiety with the $[Pt_2(\mu\text{-}Ph_2PNPPh_2)_2(C{\equiv}CC_6H_4R\text{-}p)_4]^{2-}$ subunit. This pulls the two Pt^{II} atoms into close proximity as a result of the reduced donating capability of the acetylides upon π-coordination with Ag^I centers. The short Ag–Ag (3.18–3.33 Å) and Ag–Pt distances (2.90–2.94 Å) suggest the presence of strong intermetallic contacts. Deprotonation of PPh_2NHPPh_2 in **29** and **30** is distinctly reflected by the significantly shortened P–N distances (1.59–1.63 Å) compared with those (1.68–1.73 Å) in the parent $[Ag_2(\mu\text{-}PPh_2NHPPh_2)_3](BF_4)_2$ [63].

In addition to ligand-centered high-energy absorptions below 300 nm, the UV–vis electronic spectra of Pt_2Ag_4 complexes exhibit two low-energy absorption bands at 340–400 and ca. 485 nm in acetonitrile solution. Upon excitation at $\lambda_{ex} > 320$ nm, both solid-state and solution samples of the Pt_2Ag_4 species exhibit intense room-temperature luminescence. As shown in Fig. 10, the Pt_2Ag_4 complexes in fluid acetonitrile solutions at 298 K gave a low-energy emission at ca. 711 nm for **29** and 682 for **30** (Fig. 10) with lifetimes in the microsecond range (Table 3). The blue-shifted luminescence from **29** to **30** coincides with the higher π* energy level in the 4-methylphenylacetylide (**30**) relative to that in the phenylacetylide (**29**). The emissive origin is thus ascribed to the Pt_2Ag_4 cluster to acetylide $^3[Pt_2Ag_4 \rightarrow RC{\equiv}C^-]$ MMLCT triplet state modified by the short Pt–Pt and Pt–Ag contacts [55–57].

3.1.2. Pt^{II}–M^I (M = Cu, Ag, Au) alkynyl complexes based on $[M_2(\mu\text{-dppm})_2]^{2+}$

When $[M_2(\mu\text{-dppm})_2(MeCN)_2]^{2+}$ (M = Cu^I, Ag^I) or $[M_2(\mu\text{-dppm})_2]^{2+}$ (M = Au^I) is used in place of $[Ag_2(\mu\text{-}PPh_2NHPPh_2)_2(MeCN)_2]^{2+}$, the reactions with $[Pt(C{\equiv}CR)_4]^{2-}$ (R = C_6H_5, 4-$CH_3C_6H_4$, 4-$OCH_3C_6H_4$, 4-$Bu^tC_6H_4$, Bu^t, $SiMe_3$) caused isolation of PtM (**31**–**39**.), PtM_2 (**40**–**42**), and Pt_2M_3 (**43**) complexes with different nuclearity depending on the solvents and solution concentrations [64]. The ^{31}P NMR spectra of these Pt–M heteropolynuclear complexes has characteristic P satellite peaks due to the occurrence of significant Pt–P coupling with the J_{Pt-P} = 1200–1300 Hz. [64]. In the Pt–Ag species, the P donors bonded to the Ag^I centers exhibit doublets or doublet of doublets caused by both Ag–P and P–P coupling. In the Pt–Cu or Pt–Au complexes, the P donors bound to the Cu^I or Au^I centers exhibit singlets or triplets induced by the P–P coupling through P–CH_2–P and/or P–Pt–P pathways.

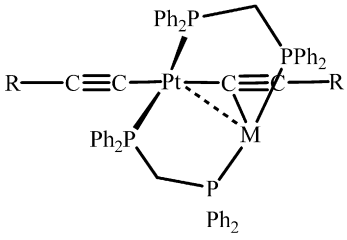

M = Ag, R = C_6H_5 **31**
M = Ag, R = $C_6H_5CH_3$-4 **32**
M = Ag, R = $C_6H_5OCH_3$-4 **33**
M = Ag, R = Bu^t **34**
M = Cu, R = C_6H_5 **35**
M = Cu, R = $C_6H_5CH_3$-4 **36**
M = Cu, R = $C_6H_5OCH_3$-4 **37**
M = Cu, R = Bu^t **38**
M = Au, R = C_6H_5 **39**

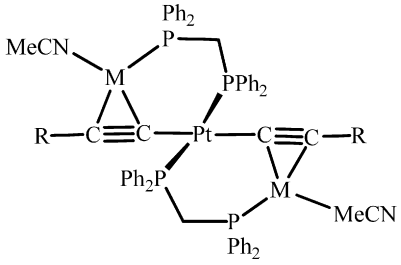

M = Ag, R = C_6H_5 **40**
M = Cu, R = C_6H_5 **41**
M = Cu, R = $SiMe_3$ **42**

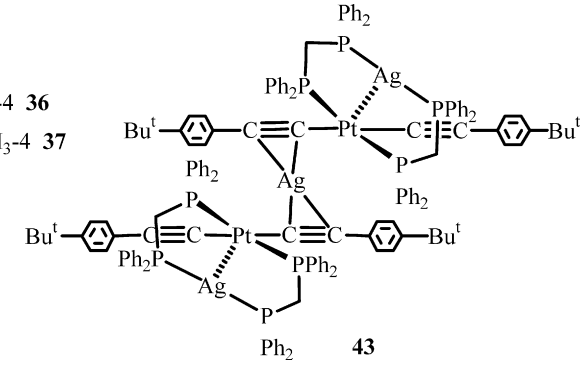

43

The PtM complexes **31**–**39** exhibit a heterobinuclear array with doubly bridging dppm. Of the two acetylides, one adopts asymmetric $\mu\text{-}\eta^1,\eta^1$ mode bonded to both Pt^{II} and M^I centers whereas the other is only bound to the Pt center in η^1 fashion. In contrast to the quasi-linear Pt–C≡C arrays, the M–C≡C arrays are curved. The short-intramolecular Pt–M distances (2.70–3.00 Å) demonstrate the occurrence of quite strong intermetallic contacts. For the PtM_2 complexes **40**–**42**, the Pt^{II} and M^I centers are bridged singly by two *anti*-arranged dppm ligands to give a quasi-linear heterotrinuclear array. The acetylide exhibits an $\mu\text{-}\eta^1,\eta^2$ bonding mode bound to the Pt^{II} center through $\sigma(\eta^1)$ and to the Cu^I centers through $\pi(\eta^2)$ coordination. The long intramolecular Pt···M (>3.4 Å) distances exclude the metallophilic contacts. The Pt_2Ag_3 heteropentanuclear complex **43**

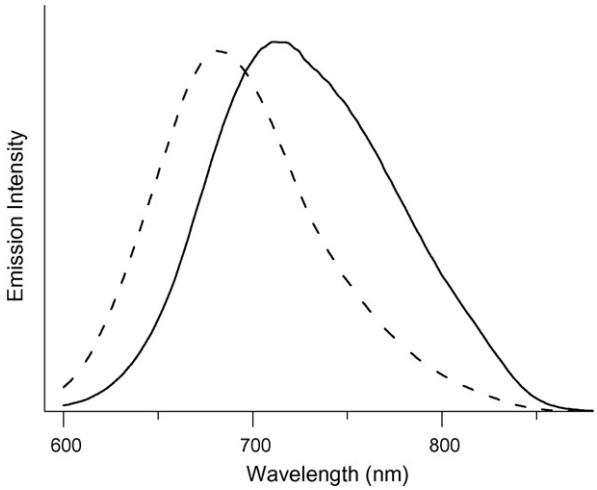

Fig. 10. Emission spectra of **29** (solid) and **30** (dashed) in fluid acetonitrile at 298 K.

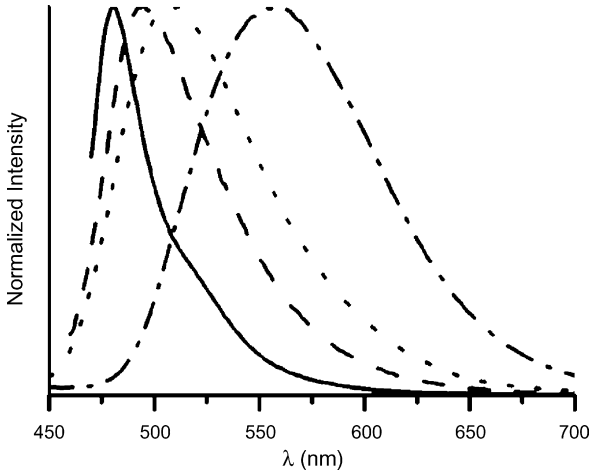

Fig. 11. Emission spectra of the PtAg heterobinuclear complexes **31** (solid), **32** (dash), **33** (dot), and **34** (dot dash) in the solid states at 298 K [64].

is derived from incorporating two PtAg subunits with one Ag^I ion through acetylide $\eta^2(\pi)$-bonding [64]. The acetylides adopt two types of bonding modes, one being μ-η^1,η^2 mode bound to the Pt^{II} center through $\sigma(\eta^1)$ and to the Ag^I centers via $\pi(\eta^2)$ coordination, whereas the other is only η^1-bonded to the Pt^{II} center. Two Pt–Ag (3.00 Å) distances imply a strong Pt–Ag contact while the other two (3.59 Å) exclude the possibility of Pt–Ag interaction.

The UV–vis absorption spectra (Table 3) of Pt–M heteropolynuclear species **31**–**43** in dichloromethane are characterized by intense absorption bands at ca. 230–280 nm, absorption shoulders at 310–350 nm and low-energy bands at ca. 365–405 nm assigned to dppm-centered, metal-perturbed $\pi \rightarrow \pi^*$ (C≡CR), and [[d(Pt) $\rightarrow \pi^*$(C≡CPh)] MLCT transitions, respectively [64]. The low-energy MLCT absorption (Table 3) in the Pt–M species with R = aryl is obviously red-shifted compared with that in the corresponding counterparts with R = alkyl due to the better π-electron-accepting capability of the former. Furthermore, the low-energy absorption displays obviously negative solvatochromism, i.e., a higher absorption energy in a more polar solvent.

The solid samples of PtM heterobinuclear species **31**–**39** luminesce strongly with lifetimes in the microsecond range at 298 K (Table 3), originating likely from [RC≡C $\rightarrow$ PtM)] LMMCT (ligand to metal–metal charge transfer) triplet states in view of the short Pt···M contacts [64]. The emission energy is **31** > **32** > **33** > **34** (Fig. 11) for the PtAg species and **35** > **36** > **37** > **38** for the PtCu complexes (Table 3), which accords well with the R electron-donating capability in the RC≡C ligands ($C_6H_5 < C_6H_4CH_3$-4 < $C_6H_4OCH_3$-4 < Bu^t). As indicated in Fig. 11, with systematic variation of the R substituents in the alkynyl (RC≡C) ligands, luminescence in the PtCu heterobinuclear complexes is progressively red-shifted and the emission color tunable with λ_{em} = 481 nm (blue) for **31**, 495 nm (cyan) for **32**, 512 nm (green) for **33** and 558 nm (yellow) for **34**.

In degassed dichloromethane at 298 K, the PtAg complexes **31**–**34** (Table 3) display a dual emission, where the higher energy (λ_{em} = 410–440 nm) emission, with lifetimes in the nanosecond range, is from ligand-centered fluorescence, whereas the low-energy emission (λ_{em} = 525–550 nm) with lifetimes in the microsecond range is probably associated with a triplet excited state. The PtCu complexes, however, only show the high-energy emission at ca. 415–455 nm with lifetimes in the nanosecond range in degassed dichloromethane solutions.

The PtM_2 complexes **40**–**42** (Table 3) exhibit intense room-temperature luminescence in both the solid state and fluid solutions, originating probably from [RC≡C $\rightarrow$ PtM_2)] LMCT transition. Because the electron-donating ability is $C_6H_5 < SiMe_3$ in the acetylide ligands, a notable red shift of the emission occurs from the **41** (R = C_6H_5) to **42** (R = $SiMe_3$). The Pt_2Ag_3 species **43** (Table 3) is strongly phosphorescent in the solid state (λ_{em} = 576 nm at 298 K) and in frozen dichloromethane (λ_{em} = 543 nm) at 77 K, but only affords moderate fluorescence at ca. 437 nm with the lifetime τ_{em} = 3.2 ns in dichloromethane at 298 K. The solid-state phosphorescence is significantly red-shifted compared with that of the PtAg heterobinuclear species because formation of the Pt_2Ag_3 heteropentanuclear array would favor reducing the energy gap between the HOMO and LUMO orbitals so that the contribution from the metal-centered transition is remarkably enhanced.

3.2. d^{10}–d^{10} heteropolynuclear alkynyl complexes

Because of the bonding versatility and structural complexity of the coinage metal acetylides, many group **11** homonuclear cluster complexes were prepared and characterized structurally [14–17]. Recent development in coinage metal acetylide complexes has been highly stimulated by their attractive optical properties and potential applications as molecular level optoelectronic materials [14,19]. The group **11** homonuclear acetylide complexes, isolated by reactions of $[M_2(\mu\text{-}Ph_2PXPPh_2)_2(MeCN)_2]^{2+}$ (X = CH_2 or NH; M = Cu^I, Ag^I or Au^I) with alkynyl or depolymerizing polymeric group **11** metal acetylides by phosphines, always exhibit intriguing luminescent properties [14,19].

Due to synthetic difficulty in controlling the heteropolynuclear arrays, the chemistry of d^{10}–d^{10} heteropolynuclear coinage metal alkynyl complexes has been comparatively neglected so that the number of heteropolynuclear alkynyl complexes are, to date, rather limited [21,65–68]. Abu-Salah [21] described the preparation of a series of group **11** hetermetallic acetylide cluster complexes with various nuclearity and structural complexity by reactions of the anionic linear phenylacetylide complexes $[M(C{\equiv}CPh)_2]^-$ (M = Cu, Ag, Au) with polymeric metal phenylacetylide species $[M(C{\equiv}CPh)]_n$. Bruce et al. [65] reported the synthesis of Cu_6Au heteroheptanuclear dumbbell species $[\{Cu_3(\mu_3\text{-}I)(\mu\text{-}dppm)_3\}_2(\mu_3{:}\mu_3\text{-}C{\equiv}CC{\equiv}CAuC{\equiv}CC{\equiv}C)]^+$ from reaction of the mononuclear $[Au(C{\equiv}CC{\equiv}CH)_2]^-$ with a trinuclear triangular cluster $[\{Cu_3(\mu\text{-}dppm)_3\}(\mu_3\text{-}I)_2]^+$. Yam et al. [66] prepared a series of Au_2Cu heterotrinuclear acetylide complexes $[\{Au(PR_3)\}\{\eta^2\text{-}C{\equiv}CC(=CH_2)Me\}_2Cu]^+$ (R = Ph, *p*-Tol) and $[(\mu\text{-dppf})Au_2\{\eta^2\text{-}C{\equiv}CC(=CH_2)Me\}_2M]^+$ (M = Cu, Ag) by reaction of metalloligands $[Au(PR_3)\{C{\equiv}CC(=CH_2)Me\}]$ and $[(\mu\text{-dppf})Au_2\{\eta^2\text{-}C{\equiv}CC(=CH_2)Me\}_2]$ with Cu^+ or Ag^+ ion through acetylide η^2-coordination. Incorporation of these metalloligands to Cu^+ or Ag^+ ion through acetylide π-coordination induces obviously red-shifted emission relative to the corresponding Au^I precursor complexes. For the $AuCu_2$ het-

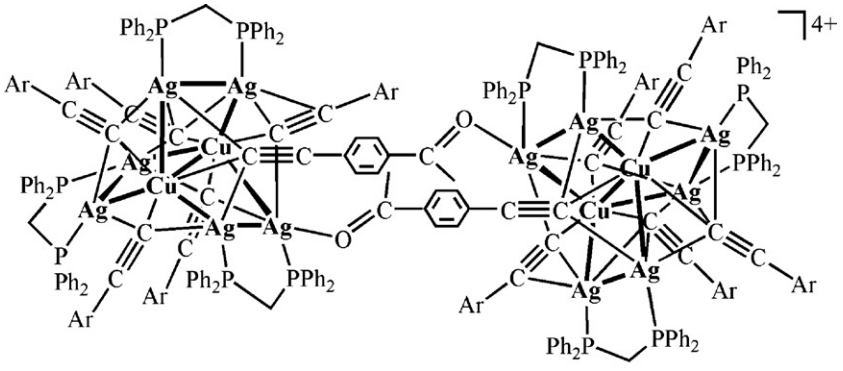

Ar = $C_6H_4C(O)CH_3$-4 **50** (see ref. 70)

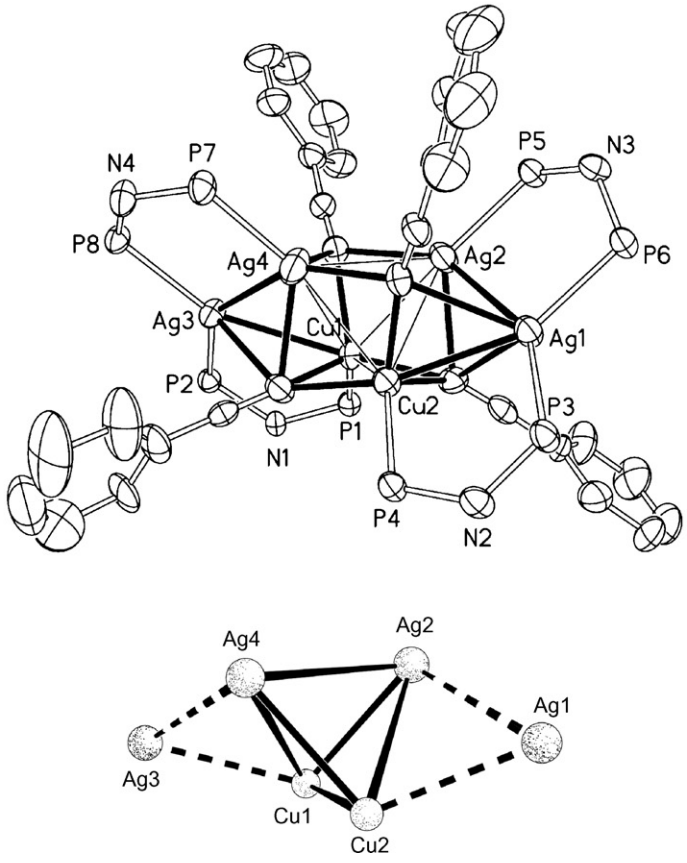

Fig. 12. ORTEP drawing (top) of **44** with atom labeling scheme showing 30% thermal ellipsoids and the structure of the Ag_4Cu_2 core (lower) [69].

erotrinuclear species with dppf, the luminescence is "turned on" when Cu^+ or Ag^+ are encapsulated into the non-emissive dppf-containing metalloligands.

For the purpose of fabricating luminescent group **11** heteropolynuclear alkynyl complexes, we have developed a feasible synthetic approach by utilizing d^{10} metal diphosphine component $[M_2(\mu\text{-}Ph_2PXPPh_2)_2(MeCN)_2]^{2+}$ (M = Cu, Ag, Au; X = NH or CH_2) to depolymerize polymeric d^{10} metal alkynyl species $(M'C{\equiv}CR)_n$ (M′ = Cu, Ag, Au; R = alkyl, aryl). By this approach, a series of d^{10}–d^{10} heteropolynuclear alkynyl cluster complexes have been accessed and their photophysical properties extensively investigated.

3.2.1. Ag^I–Cu^I heteropolynuclear alkynyl complexes

Depolymerization of silver acetylides $(AgC{\equiv}CC_6H_4R\text{-}4)_n$ (R = H, CH_3, OCH_3, NO_2, $COCH_3$) by addition of $[Cu_2(\mu\text{-}Ph_2PXPPh_2)_2(MeCN)_2]^{2+}$ (X = NH or CH_2) induced isolation of the heterohexanuclear species $[Ag_4Cu_2(\mu\text{-}Ph_2PNHPPh_2)_4(C{\equiv}CC_6H_4R\text{-}4)_4]^{2+}$ (R = H **44**, CH_3 **45**) when X = NH [69], whereas heterooctanuclear complexes $[Ag_6Cu_2(\mu\text{-}Ph_2PCH_2PPh_2)_3(C{\equiv}CC_6H_4R\text{-}4)_6(MeCN)]^{2+}$ (R = H **46**, CH_3 **47**, OCH_3 **48**, NO_2 **49**) were isolated when X = CH_2. Most remarkably, a $Ag_{12}Cu_4$ heterohexadecanuclear complex $[Ag_6Cu_2(\mu\text{-}Ph_2PCH_2PPh_2)_3(C{\equiv}CC_6H_4COCH_3\text{-}4)_6]_2^{4+}$ (**50**) was obtained for 4-acetylphenylacetylide, resulting from dimerization of the Ag_6Cu_2 species through Ag^I–O bonding interaction between Ag^I centers and acetyl O donors [69].

The Ag_4Cu_2 cluster complexes **44** (Fig. 12) and **45** display a distorted bicapped cubic skeleton ($Ag_4Cu_2C_4$) composed of four Ag^I and two Cu^I atoms and four acetylide C donors. Within the Ag_4Cu_2 hexanuclear cluster core, Cu1Cu2Ag2Ag4 forms a Cu_2Ag_2 cluster tetrahedron (Fig. 12, down). The Ag_4Cu_2 array can be regarded as a dimer of the triangular cluster subunit $[Ag_2Cu(\mu\text{-}Ph_2PNHPPh_2)_2(C{\equiv}CC_6H_4R\text{-}4)_2]^+$. The Cu^I–Cu^I distances (2.57 for **44** and 2.53 Å for **45**) are comparable to those observed in tetranuclear cubic cluster complexes $[Cu(C{\equiv}CR)(PR'_3]_4$ [70]. The rather short Cu^I–Ag^I (2.75–3.10 Å) and Ag^I–Ag^I (2.98–3.27 Å) distances suggest the presence of strong intermetallic interactions. The Ag_6Cu_2 heterooctanuclear cluster complexes **46–49** exhibit a waterwheel-like structure that can be regarded as two $Ag_3Cu(C{\equiv}CC_6H_5)_3$ subunits put together by three bridging $Ph_2PCH_2PPh_2$ as shown in Fig. 13 (**46**). The six Ag^I centers make up of a twisting triangular prism with the Cu^I atoms located at the centers of two trigonal basal planes. The acetylides adopt μ_3-η^1, μ_4-η^1 or μ_3-η^1,η^1,η^2 bonding modes to link Ag^I and Cu^I centers. The metal–metal distances (Cu^I–Cu^I = 2.96–3.42 Å, Ag^I–Cu^I = 2.60–2.83 Å, and Ag^I–Ag^I = 3.00–3.07 Å) indicate that considerable strong intermetallic contracts are operating in the Ag_6Cu_2 cluster.

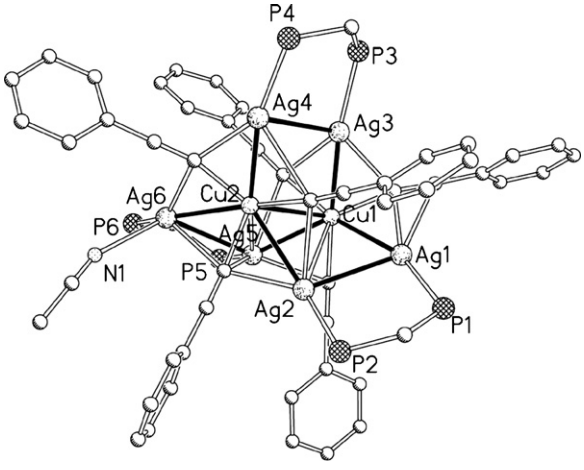

Fig. 13. Perspective view of **46** with atom labeling scheme. Phenyl rings on the phosphorus atoms are omitted for clarity [69].

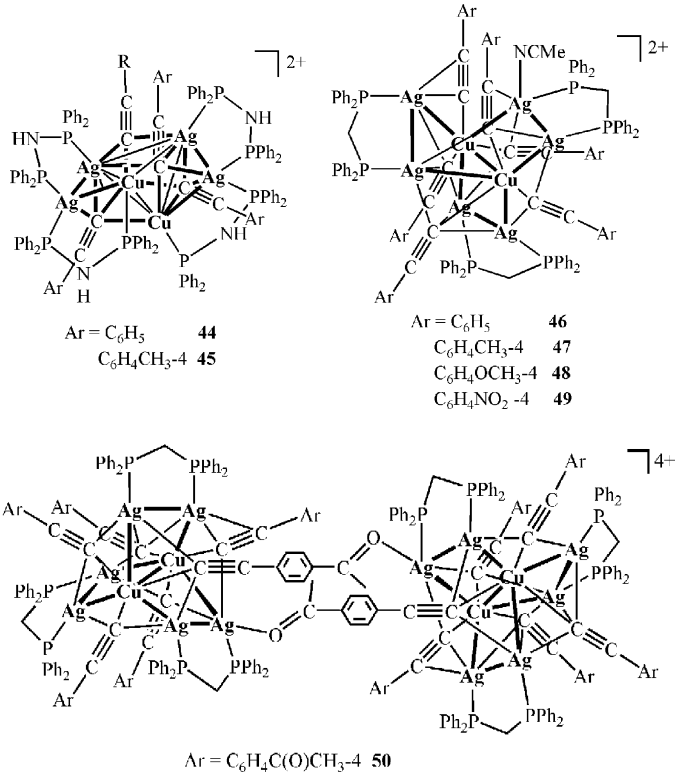

As depicted in Fig. 14, the $Ag_{12}Cu_4$ heterohexadecanuclear cluster complex **50** is a dimeric species of the Ag_6Cu_2 heteroctanuclear species through the Ag4A–O2 (2.534(4) Å) bonding between the acetyl O2A in 4-acetylphenylacetylide and the Ag4 atom. The Ag–Ag, Cu–Cu and Ag–Cu distances within each of the Ag_6Cu_2 cluster subunit are comparable to those in **46–49**. The intercluster metal···metal separations between the two Ag_6Cu_2 clusters through the bridging 4-acetylphenylacetylide, however, are >10.0 Å.

The UV–vis absorption spectra of Ag^I–Cu^I heteropolynuclear species **44–50** (Table 4) in dichloromethane solutions are characterized by intense ligand-centered bands at ca. 218–255 nm and absorption at 280–340 nm with low-energy shoulders tailing to ca. 450 nm due to metal-perturbed π–π* ($C{\equiv}CC_6H_4R$-4) transitions. Electron-deficient acetyl or nitro containing samples **49** and **50**, however, exhibit intense lower-energy absorption at ca. 350–410 nm. With excitation at $\lambda_{ex} > 350$ nm, the Ag^I–Cu^I heteropolynuclear species exhibit intense room-temperature luminescence (Table 4) both in the

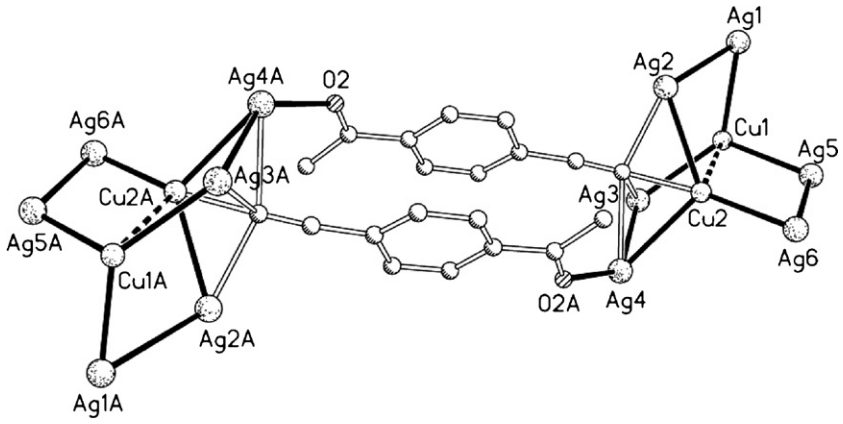

Fig. 14. A view of the dimeric $Ag_{12}Cu_4$ complex **50** showing the linkage of two Ag_6Cu_2 cluster cores through Ag–O bonding.

solid states and dichloromethane solutions, originating most likely from [acetylide → Ag_4Cu_2 or Ag_6Cu_2] ^{3}LMCT triplet transition mixed with some metal cluster-centered (d → s) character modified by strong intermetallic contacts [14,18]. The emission energy in the Ag_4Cu_2 species is **46** > **47** > **48**, according well with the σ-donating properties with phenylacetylide < 4-methylphenylacetylide < 4-methoxyphenylacetylide. **49** and **50** containing electron-deficient 4-nitrophenylacetylide or 4-acetylphenylacetylide, nevertheless, show emission at much lower energy (Table 4) compared with that in **46**–**48** because of the lowest lying excited state being dominated by an intraligand $^3[\pi \rightarrow \pi^*]$ character mixed possibly with some metal cluster-centered character [14].

3.2.2. Ag^I–Au^I heteropolynuclear alkynyl complexes

Reactions of $(AgC{\equiv}CC_6H_4R\text{-}4)_n$ with $[Au_2(\mu\text{-dppm})_2]^{2+}$ in dichloromethane produce green solutions. On one hand, metastable green Au_6Ag_{13} complexes $[Au_6Ag_{13}(\mu\text{-dppm})_3(\mu_3\text{-}\eta^1\text{-}C{\equiv}CC_6H_4R\text{-}4)_{14}]^{5+}$ (R = H **51**, CH_3 **52**, Bu^t **53**) were isolated as green crystals by layering diethyl ether onto the concentrated dichloromethane solutions with exclusion of light [71]. On the other hand, layering diethyl ether onto the acetonitrile solutions without exclusion of light, however, gave the Au_5Ag_8 products $[Au_5Ag_8(\mu\text{-dppm})_4\{\mu_5\text{-}1,2,3\text{-}C_6(C_6H_4R\text{-}4)_3\}(C{\equiv}CC_6H_4R\text{-}4)_7]^{3+}$ (R = H **51a**, CH_3 **52a**, Bu^t **53a**) as red crystals, in which photolysis caused formation of the unprecedented trianion μ_5-$\{1,2,3\text{-}C_6(C_6H_4R\text{-}4)_3\}^{3-}$ by cyclotrimerization of arylacetylide $C{\equiv}CC_6H_4R$-4 [72].

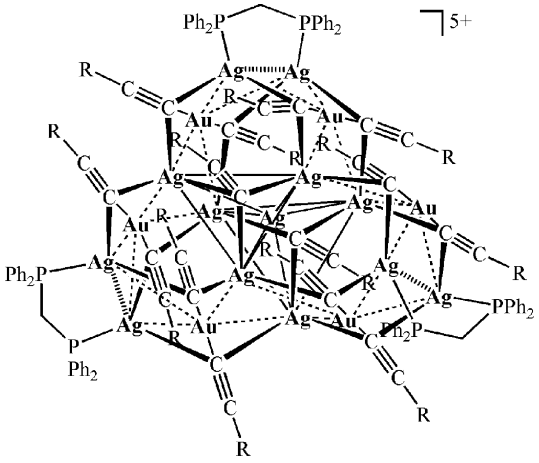

R = C_6H_5 **51**
$C_6H_4CH_3$-4 **52**
$C_6H_4Bu^t$-4 **53**

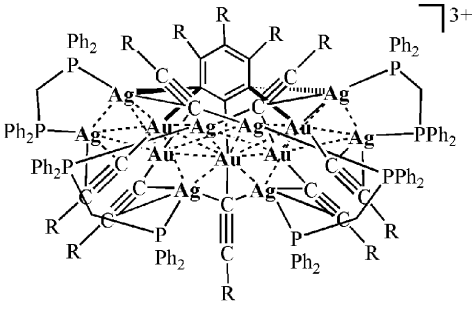

R = C_6H_5 **51a**
$C_6H_4CH_3$-4 **52a**
$C_6H_4Bu^t$-4 **53a**

The metastable green Au_6Ag_{13} species **51**–**53** (Fig. 15) display a cage structure [71]. As indicated in Fig. 15(top), three distorted hexagonal prisms (highlighted by thick lines) are intersected by sharing one rim with each other. The ligand-unsupported Ag^I atom is situated at the center of the three intersected hexagonal prisms which are symmetry-related by a C_3-axis through C51Ag5C61 atoms. Within the Au_6Ag_{13} cluster core (Fig. 15, lower), the middle part (highlighted by thick lines) is an Ag_6 triangular prism with the ligand-unsupported Ag^I atom at the center. The rather short Au^I–Ag^I (2.94–3.22 Å) and Ag^I–Ag^I (2.89–3.32 Å) distances demonstrate the presence of significant metallophilic contacts in the Au_6Ag_{13} cluster [1]. The Au···Au distances, however, are >3.50 Å. The $C{\equiv}CC_6H_4R$-4 adopt the μ_3-η^1 bonding mode, in which two of them cap symmetrically three Ag^I centers, respectively, whereas the others are bound to one Au^I and two

Table 4
Photophysical data for Ag^I–Cu^I heteropolynuclear alkynyl complexes **44**–**50**

Complexes	Medium	λ_{abs} (nm) (ε, $dm^3\ mol^{-1}\ cm^{-1}$)	λ_{em} (nm) (τ_{em}, μs) at 298 K	λ_{em} (nm) at 77 K
44	Solid		480 (1.2)	478, 525 (sh)
	CH_2Cl_2	239 (209,940), 285 (196,070)	453, 616 (sh)	464, 507 (sh)
45	Solid		483 (1.3), 531 (sh)	484, 531 (sh)
	CH_2Cl_2	239 (216,020), 302 (216,980), 331 (114,690)	458, 620 (sh)	468, 515 (sh)
46	Solid		478 (5.6)	478, 524 (sh)
	CH_2Cl_2	256 (44,160), 288 (39,660), 322 (33,780)	458	467
47	Solid		484 (5.1), 600 (sh)	481, 533 (sh)
	CH_2Cl_2	263 (46,190), 320 (50,050), 343 (35,180)	463	464, 505 (sh)
48	Solid		498 (1.5), 606	579
	CH_2Cl_2	256 (80,930), 321 (66,910), 335 (50,110)	546	463, 502 (sh)
49	Solid		601 (3.4)	610
	CH_2Cl_2	266 (42,550), 368 (33,380), 410 (29,170)	534	574
50	Solid		532 (1.8)	526
	CH_2Cl_2	256 (51,600), 304 (74,890), 360 (59,530), 389 (40,800)	516	525

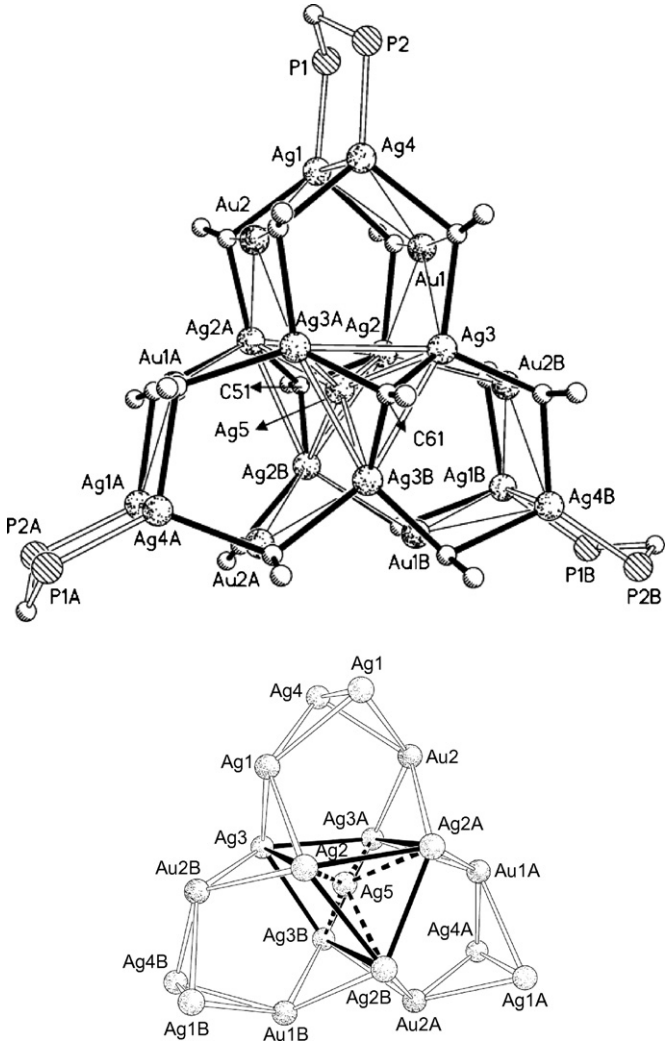

Fig. 15. Perspective view of **52** with atom labeling scheme (top) and the Au_6Ag_{13} cluster core structure (lower) [71].

Ag^I centers in an asymmetric mode.The red Au_5Ag_8 species **51a**–**53a** [72] consist of five Au^I and eight Ag^I centers linked together by bridging dppm, phenylacetylide $^-C{\equiv}CC_6H_5$ and tri-anion $\{1,2,3\text{-}C_6(C_6H_5)_3\}^{3-}$ as depicted in Fig. 16. The Au–Ag (2.70–3.10 Å) and Ag–Ag (3.10–3.20 Å) distances are comparable to those in the metastable green Au_6Ag_{13} cluster species

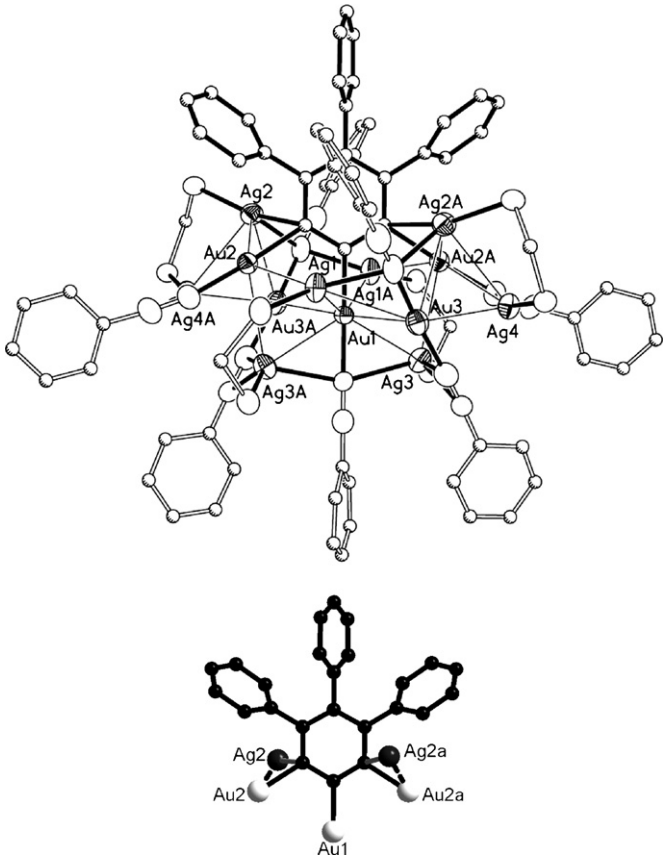

Fig. 16. Perspective view of **51a** with atom labeling scheme (top) and a view of μ_5-$\{1,2,3\text{-}C_6(C_6H_5)_3\}^{3-}$ coordination (lower), showing the two *anti*-oriented Ag–C_{aryl} bonds [72].

51–53 [71]. The intramolecular Au–Au distance, nevertheless, are shortened significantly upon formation of stable red Au_5Ag_8 species (Au–Au = 3.10–3.35 Å) by photolysis of metastable green Au_6Ag_{13} cluster complexes (Au···Au > 3.5 Å). The phenylacetylides adopt either μ_3-$\eta^1(\sigma)$ or μ-$\eta^1(\sigma)$,$\eta^2(\pi)$ bonding mode. The trianion $\{1,2,3\text{-}C_6(C_6H_5)_3\}^{3-}$ displays an unusual μ_5-bonding mode bound to three Au^I and two Ag^I centers as shown in Fig. 16 (lower). The three Au–C_{aryl} bonds are almost coplanar with the trianionic phenyl ring, whereas the two Ag–C_{aryl} bonds are *anti*-oriented, in which Ag2 and Ag2a are located up and down this phenyl ring ca. 2.40 Å, respectively.

The UV–vis absorption spectra of green Au_6Ag_{13} species **51–53** (Table 5) in dichloromethane are characterized by high-energy ligand-centered absorption at ca. 250–320 nm and shoulders at ca. 350 nm tailing to 500 nm, arising from metal-perturbed $\pi \rightarrow \pi^*$ (C≡C) transitions. With excitation at $\lambda > 350$ nm, they emit bright green luminescence (λ_{em} = 520–570 nm) both in the solid states and solutions at room temperature with quantum yields Φ_{em} being 0.025–0.112 (Table 5) in degassed fluid dichloromethane solutions. Because typically vibronic-structured emission bands relevant to the acetylides in the excited states are unobserved, the emission origin is most likely dominated by a metal-cluster-centered (d → s) triplet states modified by metal–metal contacts.

The UV–vis spectra of red Au_5Ag_8 species **51a–53a** (Table 5) are characterized by high-energy absorption at 230–90 nm and low-energy bands at ca. 365 and 440 nm. With excitation at $\lambda_{ex} > 350$ nm, they emit red luminescence (λ_{em} = 630–680 nm) both in the solid states and fluid solutions (Table 5). The emission intensity, however, is much weaker than that of the corresponding Au_6Ag_{13} species **51–53** with $\Phi_{em} < 0.005$ in degassed dichloromethane solutions.

Interestingly, metastable green Au_6Ag_{13} complexes **51–53** can be gradually photolyzed into red Au_5Ag_8 species **51a–53a** with occurrence of silver precipitate. It is postulated that light irradiation of the green Au_6Ag_{13} species induces $Ag^+ \rightarrow Ag$ to occur as well as to produce free radicals necessary for formation of $\{\mu_5\text{-}1,2,3\text{-}C_6(C_6H_4R\text{-}4)_3\}^{3-}$ by cyclotrimerization of arylacetylide. It is well known that cyclotrimerization of substituted alkynes usually gives 1,3,5- or/and 1,2,4-trisubstituted benzene derivatives in high selectivity. To our knowledge, isolation of 1,2,3-trisubstituted counterparts by this approach, however, has been attained in a few cases with extreme low yields (<8%) [73–75]. Photolysis of metastable green Au_6Ag_{13} complexes into stable red Au_6Ag_{13} species is undoubtedly unusual, inducing formation of 1,2,3-trisubstituted benzene derivatives in high selectivity by cyclotrimerization of arylacetylide. It is assumed that photolysis of the green metastable Au_6Au_{13} species (**51–53**) is likely involved in formation of Dewar benzene intermediates (Scheme 4) from cyclotrimerization of arylacetylides, which can be gradually transformed into the red Au_5Au_8 species (**51a–53a**). As shown in Fig. 17, this conversion process can be monitored by irradiation of the dichloromethane solution of metastable Au_6Au_{13} species **52** with a xenon lamp at λ = 440 nm. With the green (Au_6Au_{13} species) solution transforming into red (Au_5Au_8 species) solution, the emission at 560 nm

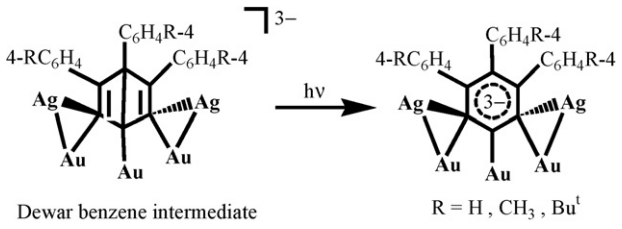

Scheme 4.

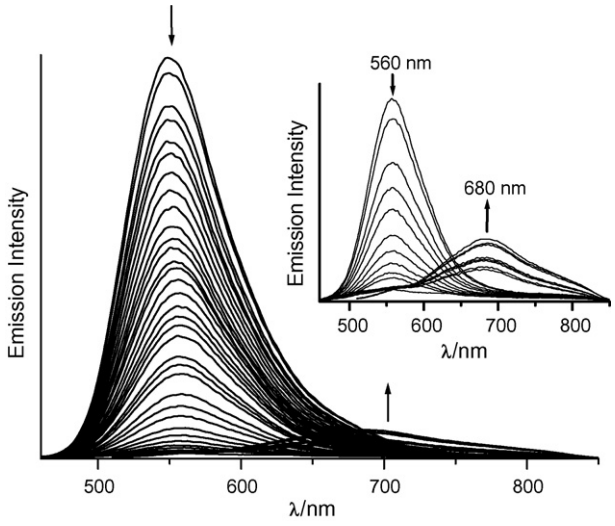

Fig. 17. Emission spectra of **52** in degassed dichloromethane upon continual irradiation with a xenon lamp at 440 nm, showing the emission decay of metastable Au_6Au_{13} species at 560 nm and the emission grow of stable Au_5Au_8 species at 680 nm during the photolysis [71].

decays rapidly whereas that at 680 nm gradually enhances [71].

3.2.3. Ag^I–M^I (M = Cu, Ag, Au) heteropolynuclear complexes of ferrocenylethynyl

In contrast with the general alkyl- or arylethynyls, ferrocenylethynyl (FcC≡CH) is redox-active and widely used in design of the molecules with [D]–[M]–[A] ([D] = donor, [M] = metal or cluster, [A] = acceptor) arrays [76,77]. Depolymerizing polymeric silver ferrocenylacetylide $(AgC{\equiv}CFc)_n$ using d^{10} metal diphosphine species $[M_2(Ph_2PXPPh_2)_2(MeCN)_2]^{2+}$ induced isolation of octahedral homohexanuclear Ag_6^I and Cu_6^I complexes when X = CH_2 [78]. When X = NH, however, the reaction gave rhombic dodecahedral heterometallic $Ag^I{}_8M^I{}_6$ (M = Cu, Ag, Au) cage complexes together with a 1,2,5-azadiphospholium product as indicated in Scheme 5 [79].

The 1,2,5-azadiphospholium species $[FcC{=}CH(Ph_2PNPPh_2)]^+$ (**54**) is derived from cyclic addition of ferrocenylethynyl with PPh_2NHPPH_2. The sp^2-hybridization in Fc–C=CH (126.6(4)°) is reflected by the C=C (1.341(6) Å) double bonding character as well as the strong ν(C=C) vibration at 1618 cm^{-1} in the IR spectrum. The P–N (1.601(4) and 1.612(4) Å) distances are comparable to those in the deprotonated $[Ph_2PNPPh_2]^-$ (1.59–1.63 Å) [62], but obviously shorter than those in PPh_2NHPPH_2 (1.68–1.73 Å) [63].

Table 5
Photophysical data for Ag^I–Au^I heteropolynuclear alkynyl complexes **51**–**53a**

Complex	Medium	λ_{abs} (nm) (ε, $dm^3\ mol^{-1}\ cm^{-1}$)	λ_{em} (nm) (τ_{em}, μs) at 298 K	Φ_{em}[a]	λ_{em} (nm) at 77 K
51	Solid		525 (0.05)		536
	CH_2Cl_2	249 (80,820), 304 (76,440), 348 (53,980), 600 (520)	545 (0.55)	0.025	531
52	Solid		545 (0.41)		562
	CH_2Cl_2	248 (71,880), 304 (69,710), 320 (69,660), 357 (56,680), 610 (1750)	560 (5.66)	0.112	557
53	Solid		523 (0.04)		540
	CH_2Cl_2	250 (78,970), 304 (76,650), 320 (77,450), 352 (59,770), 610 (2510)	546 (0.80)	0.032	539
51a	Solid		638 (0.50)		659, 608(sh)
	CH_2Cl_2	232 (258,240), 364 (58,850), 440 (29,930)	651 (<0.1)		632
52a	Solid		630 (0.23)		655, 610(sh)
	CH_2Cl_2	229 (274,490), 287 (161,200), 365 (61,600), 443 (32,840)	642 (<0.1)		632
53a	Solid		634 (0.35)		652, 608(sh)
	CH_2Cl_2	232 (278,560), 288 (178,370), 368 (68,070), 434 (40,310)			642

[a] The emission quantum yields were measured at 298 K in degassed dichloromethane solution and estimated relative to $Ru(bpy)_3(PF_6)_2$ in acetonitrile ($\Phi_{em} = 0.062$) as reference.

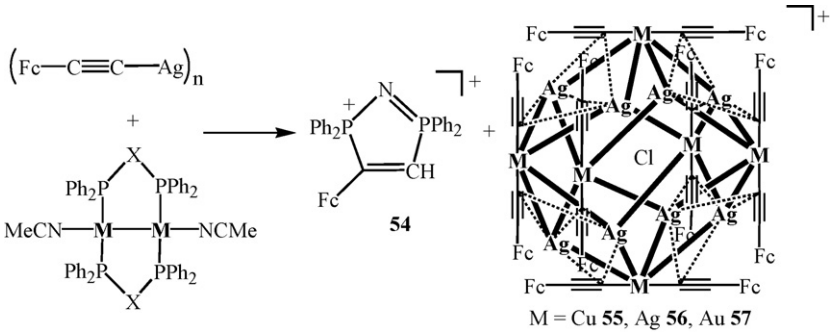

Scheme 5. Synthetic routes to **54**–**57** [79].

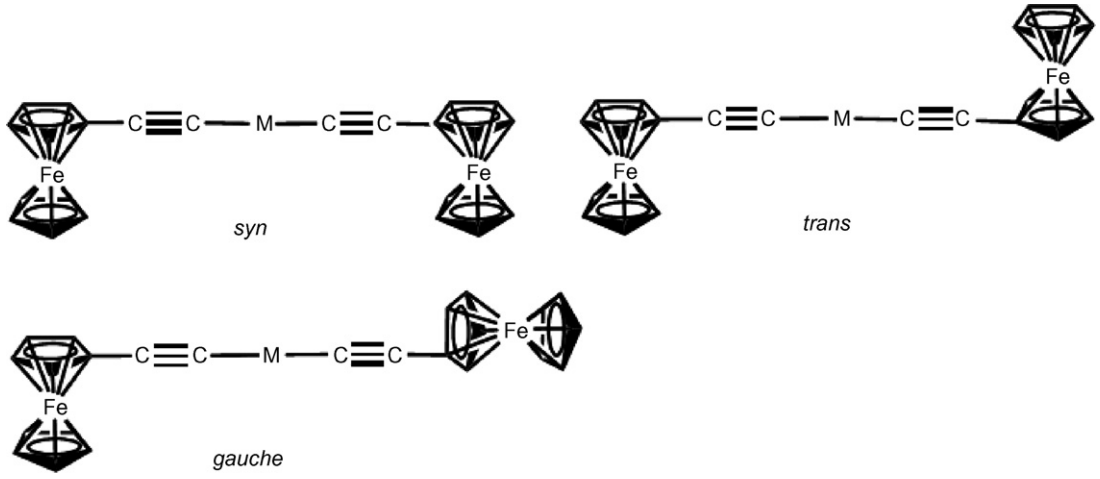

Fig. 19. Three conformations for the Fc–C≡C–M–C≡C–Fc arrays [79].

The Ag_8M_6 (M = Cu **55**, Ag **56**, Au **57**) cluster complexes consist of eight Ag^I and six M^I (M = Cu **55**, Ag **56**, Au **57**) atoms linked by twelve ferrocenylacetylides to give a cage structure with a chloride ion at the cage center. As indicated in Fig. 18, the Ag_8M_6 cluster forms a rhombic dodecahedron [80] composed of fourteen Ag_2M_2 quadrangles, in which each Ag^I atom is bound to three adjacent M^I atoms whereas each M^I atom is connected to four adjacent Ag^I atoms through strong Ag^I–M^I interactions. The acetylides adopt an asymmetric μ_3-η^1 or μ_3-η^1,η^1,η^2 bonding mode. The Fc–C≡C–M–C≡C–Fc arrays can be oriented in

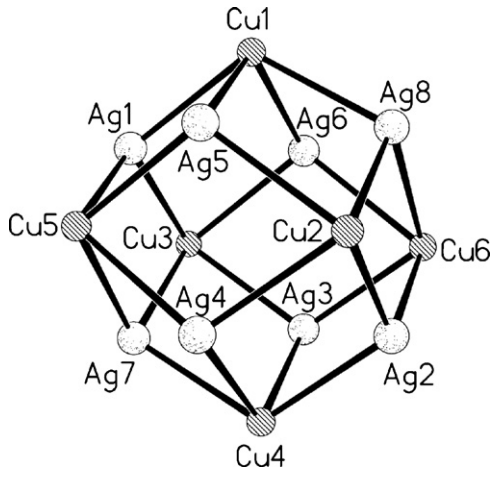

Fig. 18. View of the Ag_8Cu_6 cluster core of **55**, showing a rhombic dodecahedral structure.

three forms (Fig. 19). In contrast with the only *trans*-form in Ag_{14} complex **56** and Ag_8Au_6 complex **57**, both *cis*- and *gauche*-forms occur in Ag_8Cu_6 complex **55**. Average Fe···Fe distances in the bridging Fc–C≡C–M–C≡C–Fc arrays are 11.55 Å for **55** (M = Cu), 12.28 Å for **56** (M = Ag), and 12.25 Å for **57** (M = Au).

Although **54**–**57** are non-luminescent because the electron-donating character of ferrocenyl always quenches the emission through an electron transfer mechanism, they exhibit intriguing redox properties. **54** affords a reversible redox wave at $E_{1/2} = 0.34$ V (vs. Fc^+/Fc) which is 0.20 V positive-shifted relative to that of the ferrocenylethynyl (0.14 V). The Ag_8Cu_6 complex **55** exhibits two separate reversible redox waves (0.29 and 0.14 V) due to intramolecular electronic communication between Fc groups mediated across the quasi-linear array Fc–C≡C–Cu–C≡C–Fc. Furthermore, redox wave splitting in **55** ($\Delta E_{1/2} = 0.148$ V, Fe···Fe = 11.60 Å) is much more remarkable than those in tri- and hexanuclear Cu^I or Ag^I cluster complexes of ferrocenylethynyl [78,81] due probably to the better linearity of Fc–C≡C–M–C≡C–Fc arrays in **55**, which facilitates electron interaction to occur between the Fc groups. The redox processes of **56** and **57**, however, are irreversible owing to instability of the Ag_8M_6 (M = Ag or Au) cluster species during electrochemical measurement.

4. Concluding remarks

The incorporation of d^8/d^{10} metal thiolate/alkynyl species with d^{10} metal diphosphine units is a feasible approach for the design of group **10** and **11** heteropolynuclear thiolate/alkynyl complexes. Depending on the nature of the d^8/d^{10} metal components and the ligands as well as the reaction conditions such as solvents and concentrations, a series of d^8–d^{10} or d^{10}–d^{10} heteropolynuclear species with diverse nuclearity and structural topology have been attained. The versatile bonding character of d^8/d^{10} metal thiolates or acetylides usually favors formation of ligand-linked or -unsupported intermetallic contacts which exert a significant influence on the spectroscopic properties and the emission features of these d^8/d^{10}–d^{10} heterometallic cluster complexes. They always show intense room-temperature luminescence with a wide range of colors and lifetimes in the microsecond range in the solid state. In most cases, they also luminesce strongly in degassed fluid solution with manifold emissive origins due to MLCT, LMCT and LLCT triplet excited states mixed with some metal cluster-centered character modified by metal–metal contacts. The luminescence energy and lifetime together with their emissive origins are tunable by modifying the metal ions and the ligands as well as introducing electron-donating or -accepting substituents to the aromatic rings. A wide range of emission or color has been achieved for the square planar Pt^{II} chromophores with tunable emission energy by altering the HOMO–LUMO energy gap. These emissive d^8/d^{10}–d^{10} multicomponent and heteropolynuclear complexes may have extensive applications in organic light-emitting diodes and other molecular level optoelectronic materials.

Acknowledgements

This work was financially supported by the NSFC (20490210, 20521101, 20625101 and 20773128), the 973 project (2007CB815304) from MSTC, the NSF of Fujian Province (E0420002), and the fund from CAS.

References

[1] P. Pyykkö, Chem. Rev. 97 (1997) 597.
[2] P.C. Ford, A. Vogler, Acc. Chem. Res. 26 (1993) 220.
[3] C. Kutal, Coord. Chem. Rev. 99 (1990) 213.
[4] D. Max Roundhill, H.B. Gray, C.M. Che, Acc. Chem. Res. 22 (1989) 55.
[5] M.C. Gimeno, A. Laguna, Chem. Rev. 97 (1997) 511.
[6] M. Vitale, P.C. Ford, Coord. Chem. Rev. 219–221 (2001) 3.
[7] C.-M. Che, S.-W. Lai, Coord. Chem. Rev. 249 (2005) 1296.
[8] D.L. Phillips, C.-M. Che, K.H. Leung, Z. Mao, M.-C. Tse, Coord. Chem. Rev. 249 (2005) 1476.
[9] P.C. Ford, E. Cariati, J. Bourassa, Chem. Rev. 99 (1999) 3625.
[10] W. Paw, S.D. Cummings, M.A. Mansour, W.B. Connick, D.K. Geiger, R. Eisenberg, Coord. Chem. Rev. 171 (1998) 125.
[11] C.W. Liu, R.J. Staples, J.P. Fackler, Coord. Chem. Rev. 174 (1998) 147.
[12] J.A. Zuleta, J.M. Bevilacqua, R. Eisenberg, Coord. Chem. Rev. 111 (1991) 237.
[13] V.W.-W. Yam, C.-L. Chan, C.-K. Li, K.M.-C. Wong, Coord. Chem. Rev. 216–217 (2001) 173.
[14] V.W.-W. Yam, K.K.-W. Lo, K.M.-C. Wong, J. Organomet. Chem. 578 (1999) 3.
[15] R. Nast, Coord. Chem. Rev. 47 (1982) 89.
[16] H. Lang, K. Köhler, S. Blau, Coord. Chem. Rev. 143 (1995) 113.
[17] T.C.W. Mak, X.-L. Zhao, Q.-M. Wang, G.-C. Guo, Coord. Chem. Rev. 251 (2007) 2311.
[18] V.W.-W. Yam, K.K.-W. Lo, W.K.-M. Fung, C.-R. Wang, Coord. Chem. Rev. 171 (1998) 17.
[19] V.W.-W. Yam, Acc. Chem. Res. 35 (2002) 555.
[20] K.M.-C. Wong, C.-K. Hui, K.-L. Yu, V.W.-W. Yam, Coord. Chem. Rev. 229 (2002) 123.
[21] O.M. Abu-Salah, J. Organomet. Chem. 565 (1998) 211.
[22] E.J. Fernandez, A. Laguna, J.M. Lopez-de-Luzuriaga, Dalton Trans. (2007) 1969.
[23] J. Vicente, P. González-Herrero, M. Perez-Cadenas, P.G. Jones, D. Bautista, Inorg. Chem. 46 (2007) 4718.
[24] J. Vicente, M.T. Chicote, S. Huertas, P.G. Jones, A.K. Fischer, Inorg. Chem. 40 (2001) 6193.

[25] M. Ebihara, M. Tsuchiya, M. Yamada, K. Tokoro, T. Kawamura, Inorg. Chim. Acta 231 (1995) 35.
[26] K.-T. Youm, Y. Kim, Y. Do, M.-J. Jun, Inorg. Chim. Acta 310 (2000) 203.
[27] S.D. Robertson, A.M.Z. Slawin, J.D. Woollins, Eur. J. Inorg. Chem. (2007) 247.
[28] J. Vicente, M.T. Chicote, S. Huertas, D. Bautista, P.G. Jones, A.K. Fischer, Inorg. Chem. 40 (2001) 2051.
[29] T. Konno, Bull. Chem. Soc. Jpn. 77 (2004) 627.
[30] H.-W. Xu, Z.-N. Chen, S. Ishizaka, N. Kitamura, J.-G. Wu, Chem. Commun. (2002) 1934.
[31] M.A. Mazid, M.T. Razi, P.J. Sadler, Inorg. Chem. 20 (1981) 2872.
[32] Y.-D. Chen, L.-Y. Zhang, Y.-H. Qin, Z.-N. Chen, Inorg. Chem. 44 (2005) 6456.
[33] D. Coucouvanis, S. Kanodia, D. Swenson, S.J. Chen, T. Stuedemann, N.C. Baenziger, R. Pedelty, M. Chu, J. Am. Chem. Soc. 115 (1993) 11271.
[34] F. Canales, S. Canales, O. Crespo, M.C. Gimeno, P.G. Jones, A. Laguna, Organometallics 17 (1998) 1617.
[35] C. King, J.C. Wang, M.N.I. Khan, J.P. Fackler Jr., Inorg. Chem. 28 (1989) 2145.
[36] K. Ray, T. Weyhermüller, A. Goossens, M.W.J. Craje, K. Wieghardt, Inorg. Chem. 42 (2003) 4082.
[37] (a) J.A. Zuleta, M.S. Burberry, R. Eisenberg, Coord. Chem. Rev. 97 (1990) 47;
(b) M. Hissler, J.E. McGarrah, W.B. Connick, D.K. Geiger, S.D. Cummings, R. Eisenberg, Coord. Chem. Rev. 208 (2000) 115.
[38] S.D. Cummings, R. Eisenberg, J. Am. Chem. Soc. 118 (1996) 1949.
[39] Y.-D. Chen, Y.-H. Qin, L.-Y. Zhang, L.-X. Shi, Z.-N. Chen, Inorg. Chem. 43 (2004) 1197.
[40] Y.-D. Chen, L.-Y. Zhang, L.-X. Shi, Z.-N. Chen, Inorg. Chem. 43 (2004) 7493.
[41] V.W.W. Yam, K.L. Yu, E.C.C. Cheng, P.K.Y. Yeung, K.K. Cheung, N. Zhu, Chem. Eur. J. 8 (2002) 4122.
[42] S.D. Cummings, R. Eisenberg, Inorg. Chem. 34 (1995) 2007.
[43] S. Huertas, M. Hissler, J.E. McGarrah, R.J. Lachicotte, R. Eisenberg, Inorg. Chem. 40 (2001) 1183.
[44] S. Yamazaki, A.J. Deeming, D.M. Speel, D.E. Hibbs, M.B. Hursthouse, K.M.A. Malik, Chem. Commun. 177 (1997), and references therein.
[45] I. Ara, J. Forniés, E. Lalinde, M.T. Moreno, M. Tomas, J. Chem. Soc. Dalton Trans. 2397 (1995), and references therein.
[46] L. Manojlovic-Muir, A.N. Henderson, I. Treurnicht, R.J. Puddephatt, Organometallics 8 (1989) 2055.
[47] W.-Y. Wong, G.-L. Lu, K.-H. Choi, J. Organomet. Chem. 659 (2002) 107.
[48] Q.-S. Li, F.-B. Xu, D.-J. Cui, K. Yu, X.-S. Zeng, X.-B. Leng, H.-B. Song, Z.-Z. Zhang, Dalton Trans. (2003) 1551.
[49] J. Forniés, S. Fuertes, A. Matin, V. Sicilia, E. Lalinde, M.T. Moreno, Chem. Eur. J. 12 (2006) 8253.
[50] P. Espinet, J. Forniés, F. Martinez, M. Tomas, E. Lalinde, M.T. Moreno, A. Ruiz, A.J. Welch, J. Chem. Soc. Dalton Trans. (1990) 791.
[51] I. Ara, J. Forniés, J. Gomez, E. Lalinde, M.T. Moreno, Organometallics 19 (2000) 3137.
[52] J.P.H. Charmant, J. Forniés, J. Gomes, E. Lalinde, R.I. Merino, M.T. Moreno, A.G. Orpen, Organometallics 18 (1999) 3353.
[53] B. Gil, J. Forniés, J. Gomez, E. Lalinde, A. Martin, M.T. Moreno, Inorg. Chem. 45 (2006) 7788.
[54] V.W.-W. Yam, K.-L. Yu, K.-K. Cheung, J. Chem. Soc. Dalton Trans. (1999) 2913.
[55] V.W.-W. Yam, K.-L. Yu, K.M.-C. Wong, K.-K. Cheung, Organometallics 20 (2001) 721.
[56] V.W.-W. Yam, C.-K. Hui, K.M.-C. Wong, N. Zhu, K.-K. Cheung, Organometallics 21 (2002) 4326.
[57] V.W.-W. Yam, L.-P. Chan, T.-F. Lai, J. Chem. Soc. Dalton Trans. (1993) 2075.
[58] I. Ara, J.R. Berenguer, E. Eguizabal, J. Forniés, J. Gomez, E. Lalinde, J. Organomet. Chem. 670 (2003) 221.
[59] J.R. Berenguer, J. Forniés, B. Gil, E. Lalinde, Chem. Eur. J. 12 (2006) 785.
[60] J.P.H. Charmant, J. Forniés, J. Gomez, E. Lalinde, R.I. Merino, M.T. Moreno, A.G. Orpen, Organometallics 22 (2003) 652.
[61] J. Forniés, J. Gomez, E. Lalinde, M.T. Moreno, Inorg. Chem. 40 (2001) 5415.
[62] Q.-H. Wei, G.-Q. Yin, Z. Ma, L.-X. Shi, Z.-N. Chen, Chem. Commun. (2003) 2188.
[63] E.J. Sekabunga, M.L. Smith, T.R. Webb, W.E. Hill, Inorg. Chem. 41 (2002) 1205.
[64] G.-Q. Yin, Q.-H. Wei, L.-Y. Zhang, Z.-N. Chen, Organometallics 25 (2006) 580.
[65] M.I. Bruce, B.C. Hall, B.W. Skelton, M.E. Smith, A.H. White, J. Chem. Soc. Dalton Trans. (2002) 995.
[66] V.W.-W. Yam, K.-L. Cheung, E.C.-C. Cheng, N. Zhu, K.-K. Cheung, Dalton Trans. (2003) 1830.
[67] O. Schuster, U. Monkowius, H. Schmidbaur, R.S. Ray, S. Kruger, N. Rosch, Organometallics 25 (2006) 1004.
[68] J. Vicente, M.-T. Chicote, M.M. Alvarez-Falcon, P.G. Jones, Organometallics 24 (2005) 4666.
[69] Q.-H. Wei, G.-Q. Yin, L.-Y. Zhang, L.-X. Shi, Z.-W. Mao, Z.-N. Chen, Inorg. Chem. 43 (2004) 3484.
[70] K. Osakada, T. Takizawa, T. Yamamoto, Organometallics 14 (1995) 3531.
[71] Q.-H. Wei, L.-Y. Zhang, G.-Q. Yin, L.-X. Shi, Z.-N. Chen, Organometallics 24 (2005) 3818.
[72] Q.-H. Wei, L.-Y. Zhang, G.-Q. Yin, L.-X. Shi, Z.-N. Chen, J. Am. Chem. Soc. 126 (2004) 9940.
[73] H. Dietl, H. Reinheimer, J. Moffat, P.M. Maitlis, J. Am. Chem. Soc. 92 (1970) 2276.
[74] H.G. Viehe, R. Merényi, J.F.M. Oth, P. Valange, Angew. Chem. Int. Ed. 3 (1964) 746.
[75] M. Ballester, J. Castaner, J. Riera, I. Tabernero, J. Org. Chem. 51 (1986) 1413.
[76] G.-L. Xu, R.J. Crutchley, M.C. DeRosa, Q.-J. Pan, H.-X. Zhang, X. Wang, T. Ren, J. Am. Chem. Soc. 127 (2005) 13354.
[77] A. Albinati, F.F. de Biani, P. Leoni, L. Marchetti, M. Pasquali, S. Rizzato, P. Zanello, Angew. Chem. Int. Ed. 44 (2005) 5701.
[78] Q.-H. Wei, L.-Y. Zhang, L.-X. Shi, Z.-N. Chen, Inorg. Chem. Commun. 7 (2004) 286.
[79] Q.-H. Wei, G.-Q. Yin, L.-Y. Zhang, Z.-N. Chen, Organometallics 25 (2006) 4941.
[80] D. Rais, J. Yau, D.M.P. Mingos, R. Vilar, A.J.P. White, D.J. Williams, Angew. Chem. Int. Ed. 40 (2001) 3464.
[81] J.H.K. Yip, J. Wu, K.-Y. Wong, K.P. Ho, C.S.-N. Pun, J.J. Vittal, Organometallics 21 (2002) 5292.